

## BLOOD DISORDERS

## Thrombopoietin receptor–independent stimulation of hematopoietic stem cells by eltrombopag

Yun-Ruei Kao<sup>1</sup>, Jiahao Chen<sup>1</sup>, Swathi-Rao Narayanagari<sup>1</sup>, Tihomira I. Todorova<sup>1</sup>, Maria M. Aivalioti<sup>1</sup>, Mariana Ferreira<sup>1</sup>, Pedro M. Ramos<sup>2</sup>, Celine Pallaud<sup>2</sup>, Ioannis Mantzaris<sup>3,4</sup>, Aditi Shastri<sup>3,4</sup>, James B. Bussel<sup>5</sup>, Amit Verma<sup>3,4,6</sup>, Ulrich Steidl<sup>1,3,4,6,7\*</sup>, Britta Will<sup>1,4,6,7\*</sup>

Copyright © 2018  
The Authors, some  
rights reserved;  
exclusive licensee  
American Association  
for the Advancement  
of Science. No claim  
to original U.S.  
Government Works

Eltrombopag (EP), a small-molecule thrombopoietin receptor (TPO-R) agonist and potent intracellular iron chelator, has shown remarkable efficacy in stimulating sustained multilineage hematopoiesis in patients with bone marrow failure syndromes, suggesting an effect at the most immature hematopoietic stem and multipotent progenitor level. Although the functional and molecular effects of EP on megakaryopoiesis have been studied in the past, mechanistic insights into its effects on the earliest stages of hematopoiesis have been limited. We investigated the effects of EP treatment on hematopoietic stem cell (HSC) function using purified primary HSCs in separation-of-function mouse models, including a TPO-R–deficient strain, and stem cells isolated from patients undergoing TPO-R agonist treatment. Our mechanistic studies showed a stimulatory effect on stem cell self-renewal independently of TPO-R. Human and mouse HSCs responded to acute EP treatment with metabolic and gene expression alterations consistent with a reduction of intracellular labile iron pools that are essential for stem cell maintenance. Iron preloading prevented the stem cell stimulatory effects of EP. Moreover, comparative analysis of stem cells in the bone marrow of patients receiving EP showed a marked increase in the number of functional stem cells compared to patients undergoing therapy with romiplostim, another TPO-R agonist lacking an iron-chelating ability. Together, our study demonstrates that EP stimulates hematopoiesis at the stem cell level through iron chelation–mediated molecular reprogramming and indicates that labile iron pool–regulated pathways can modulate HSC function.

## INTRODUCTION

Thrombocytopenia can result in bleeding in patients with chronic immune thrombocytopenia (ITP) (1) and causes life-threatening complications in acquired bone marrow failure syndromes, such as severe aplastic anemia (SAA) and myelodysplastic syndrome (MDS). Whereas ITP is triggered by autoimmune-directed increased destruction and reduced production of platelets (2), SAA and MDS arise from severely compromised hematopoietic stem and multipotent progenitor (MPP) compartments in the bone marrow, albeit through distinct pathomechanisms. In SAA, immature hematopoietic cells are destroyed by activated cytotoxic T cells (3), whereas MDS arises from a molecularly and functionally aberrant and dominant stem cell clone, incapable of producing fully functional mature peripheral blood cells (4). The development of therapeutic countermeasures limiting comorbidities caused by thrombocytopenia has been a clinical priority over the last several decades.

Thrombopoietin (TPO) is the primary cytokine instructing megakaryocyte (MK) progenitor expansion and differentiation through binding to the TPO receptor [TPO-R; encoded by the myeloproliferative leukemia virus oncogene (*c-MPL*)], which elicits downstream signaling and gene expression changes and increases platelet production (5). Moreover, TPO supports maintenance of hematopoietic stem cells (HSCs) by enforcing cell cycle quiescence; alternatively, it

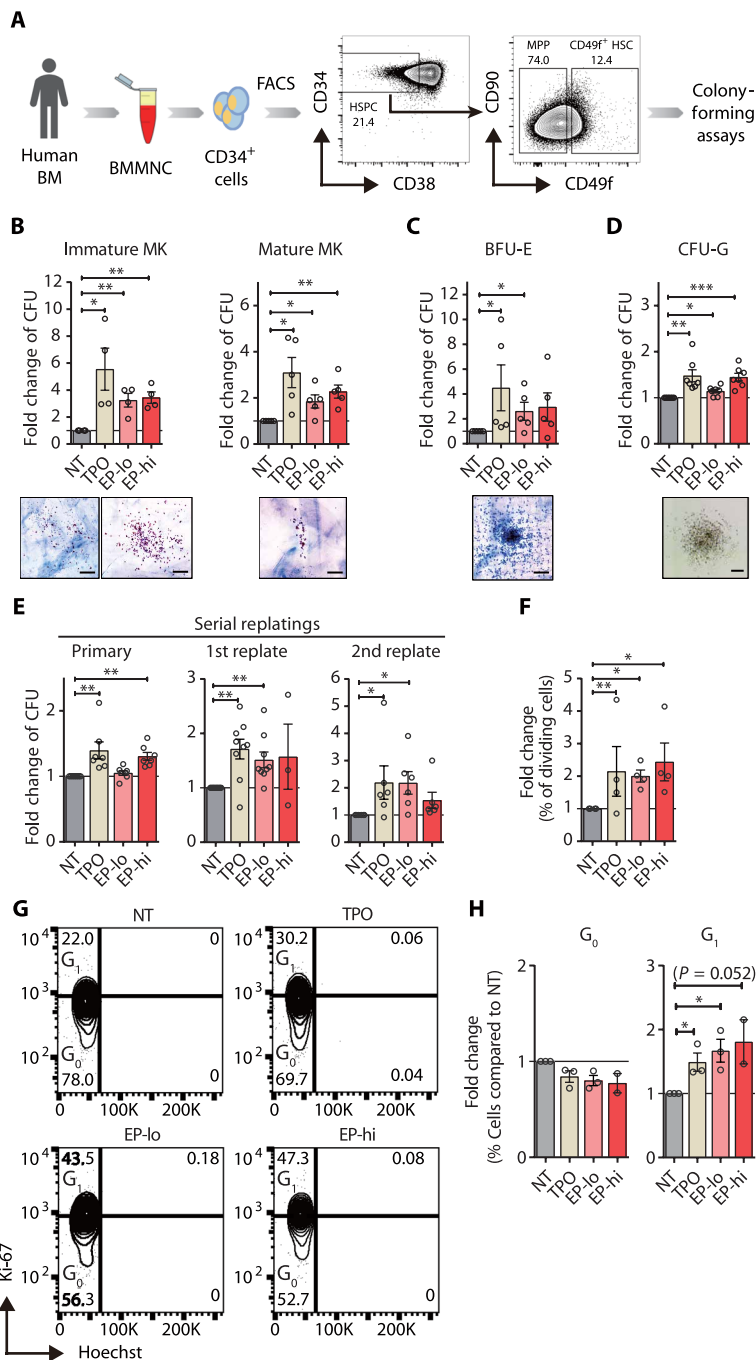
can drive stem cell differentiation commitment and increase blood cell production, aided by other cytokines (6, 7). The use and efficacy of two forms of recombinant human TPO (rhTPO) to enhance platelet production have been tested in a range of thrombocytopenic disorders (8) and have provided convincing proof-of-concept data. Unfortunately, recombinant MK growth and development factor (MGDF), a ligand for c-MPL closely related to TPO, was found to stimulate formation of drug-induced antibodies cross-reacting with endogenous TPO, which triggered severe decreases in endogenous TPO and amegakaryopoiesis (9). This prompted the abandonment of therapeutic strategies involving TPO-R stimulation through immunogenic TPO-R agonists (TPO-RAs) and led to a search for nonimmunogenic agents.

Eltrombopag (EP) is a second-generation allosteric small-molecule TPO-RA, which binds the trans- and juxta-membrane domains of the human TPO-R and robustly induces phosphorylation of signal transducer and activator of transcription 5 (STAT5), protein kinase B (AKT), and STAT3 (10, 11) in a species-specific fashion (12). Because of its noncompetitive receptor binding properties, EP can synergize with endogenous TPO in stimulating megakaryopoiesis and platelet production through enhancing cell differentiation, particularly that of immature megakaryocytic and bipotent (MK/erythrocyte) progenitor cells (11). Besides its ability to stimulate megakaryopoiesis, EP was also found to increase multilineage hematopoiesis, even upon its discontinuation in patients with acquired bone marrow failure syndromes who frequently present with increased TPO concentrations in their serum (13–16). This finding suggests that EP enhances hematopoietic stem or MPP cell function via a mechanism that is either additive or synergistic with TPO or, alternatively, in a TPO-R–independent fashion. In addition to its ability to stimulate human TPO-R signaling, EP potently chelates intracellular iron (17, 18). Although EP-mediated iron chelation was demonstrated to be functionally relevant in leukemic

<sup>1</sup>Department of Cell Biology, Albert Einstein College of Medicine, Bronx, NY 10461, USA. <sup>2</sup>Novartis Pharmaceuticals, Basel CH-4057, Switzerland. <sup>3</sup>Department of Oncology, Montefiore Medical Center, Bronx, NY 10467, USA. <sup>4</sup>Department of Medicine, Albert Einstein College of Medicine, Bronx, NY 10467, USA. <sup>5</sup>Pediatric Hematology/Oncology, Weill Cornell Medicine, New York, NY 10065, USA. <sup>6</sup>Albert Einstein Cancer Center, Albert Einstein College of Medicine, Bronx, NY 10461, USA. <sup>7</sup>Institute for Stem Cell and Regenerative Medicine Research, Albert Einstein College of Medicine, Bronx, NY 10461, USA.

\*Corresponding author. Email: britta.will@einstein.yu.edu (B.W.); ulrich.steidl@einstein.yu.edu (U.S.)

**Fig. 1. EP stimulates multilineage differentiation and self-renewal capacity of human HSCs.** (A) Scheme showing isolation of human HSCs for colony-forming assays. BM, bone marrow; HSPC, hematopoietic stem and progenitor cell. (B and C) MK (B) and erythroid (C) colony formation in collagen-based culture system ( $n = 4$ ). (D) Granulocytic colony formation in methylcellulose semi-solid medium ( $n = 7$ ). CFU, colony-forming unit; MK, MK colonies; BFU-E, burst-forming unit erythroid colonies; CFU-G, granulocyte colonies. Representative morphology for each type of colony is also shown. Scale bars, 100  $\mu$ m. (E) Colonies from primary methylcellulose cultures were serially replated biweekly ( $n = 7$ ). Results are represented as fold change of colonies compared to nontreated (NT) vehicle control (water). (F) Fold change of percentage of dividing HSCs compared to vehicle-treated control 24 hours after treatment. Percentage of dividing HSCs is expressed as the number of cells with at least one completed division out of total HSCs scored. (G) Representative fluorescence-activated cell sorting (FACS) plots of Ki-67 and Hoechst staining of HSCs ( $\text{Lin}^- \text{CD34}^+ \text{CD38}^- \text{CD49f}^+$ ) exposed to rhTPO and EP at low and high concentrations for 24 hours. (H) Quantification of percentage of cells in  $G_0$  versus  $G_1$  of cell cycle after stimulation with TPO, EP-lo, and EP-hi for 24 hours in liquid culture compared to vehicle control (NT). rhTPO, 100 ng/ml of rhTPO; EP-lo, EP (3  $\mu$ g/ml); EP-hi, EP (10  $\mu$ g/ml).  $n = 4$ . Data are means  $\pm$  SEM. \* $P < 0.05$ , \*\* $P < 0.01$ , \*\*\* $P < 0.001$  (paired Student's  $t$  test).



cells, where it induces differentiation and apoptosis (17), whether iron chelation contributes to the mechanism of action of EP in nonmalignant cells has not been investigated thus far.

Here, we investigated the functional and molecular consequences of EP treatment in HSCs. Using assays for the quantification and functional testing of primary human HSCs, we demonstrate that EP enhances stem cell self-renewal and multilineage differentiation in preclinical models, as well as in patients undergoing EP treatment. Molecular profiling of EP-treated, purified human stem cells uncovered enrichment of differentially expressed genes (DEGs) within iron-regulated pathways, suggesting an additional TPO-R-independent mechanism. Mouse HSCs lacking the TPO-R ( $c\text{-Mpl}^{-/-}$ ), comparative analysis of the functional impact of another TPO-RA lacking iron-chelating ability, and iron preloading experiments demonstrated that EP can enhance stem cell self-renewal by reducing intracellular labile iron pools (LIPs). Molecular changes in stem cells treated with EP produced compensatory responses for restoring intracellular iron concentrations and metabolic adaptations consistent with impaired glycolysis, which indicates impairment of nonenzymatic iron-dependent metabolic reactions, and an increased compensatory use of long-chain unsaturated fatty acids and amino acids in glycolytic pathways. Our data provide mechanistic insight into how EP stimulates multilineage hematopoiesis in patients with ITP even in the presence of increased TPO serum concentrations. Our findings also strongly suggest that LIPs can serve as a rheostat for HSC maintenance, a finding which is relevant to studies of tissue-specific stem cell biology, aging, and stem cell-derived malignancies.

**RESULTS**

**EP stimulates human hematopoietic stem and multilineage progenitor cells**

We first assessed the impact of EP on the functional hallmarks of primary human HSCs, which include multilineage differentiation

and self-renewal. We carried out ex vivo multilineage differentiation assays in the presence of EP using highly purified bone marrow-derived lineage-negative ( $\text{Lin}^-$ )  $\text{CD34}^+ \text{CD38}^- \text{CD49f}^+$  HSCs (Fig. 1A). Colony assays showed that EP significantly stimulated ( $P < 0.01$ ) stem cell-derived megakaryocytic colony formation compared to vehicle-treated control stem cells by two- to threefold on average (Fig. 1B). EP-treated HSCs gave rise to increased numbers of erythroid and granulocytic colonies by 2.8- and 1.4-fold, respectively (Fig. 1, C and D). We next examined ex vivo self-renewal in the presence of EP using serial replating assays and found that nearly twice as many treated stem cells retained long-term self-renewal abilities compared

Downloaded from <https://www.science.org> on August 15, 2023

to control-treated HSCs (Fig. 1E). We also evaluated the effects of EP on MPP differentiation and maintenance and found a stimulation of colony formation mostly limited to the immature megakaryocytic lineage (fig. S1, A to C). In contrast, MPPs did not show sustainably enhanced self-renewal potential upon EP treatment, compared to mock-treated progenitors (fig. S1D).

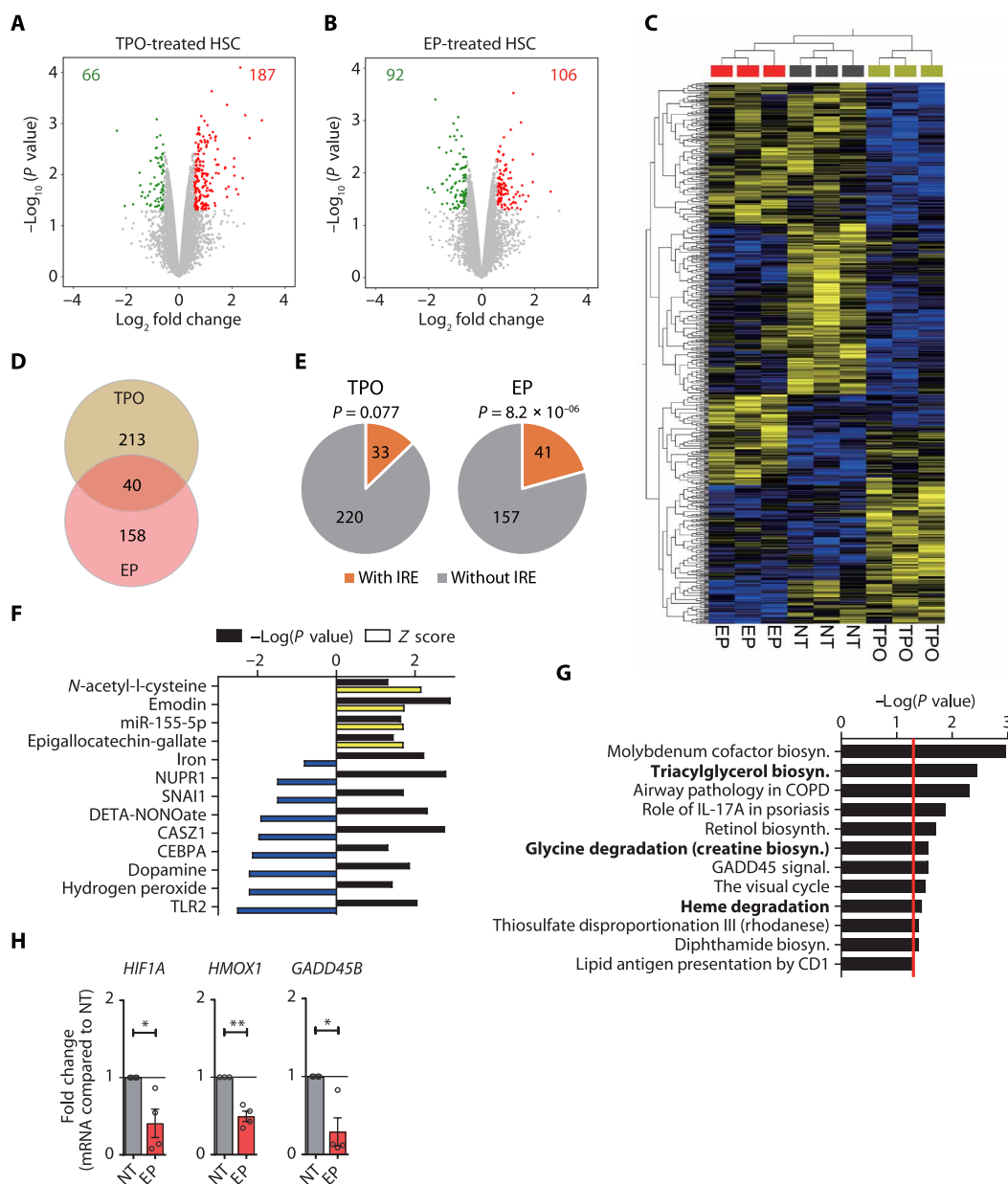
We next assessed stem cell proliferation and cell cycle status upon EP treatment. Single-cell division assays revealed that more stem cells had completed their first division within 24 hours upon treatment with EP, similar to TPO-treated controls (Fig. 1F). Cell cycle analysis of purified HSCs further showed an increase in the fraction of HSCs in active cell cycle ( $G_1$ ) upon treatment with rhTPO or EP (Fig. 1, G and H), whereas overall proliferation rates at 24 hours (fig. S2, A and B) and up to 120 hours (fig. S2, C and D) of treatment were unchanged. Together, these results indicate that EP directly

enhances multilineage hematopoiesis through increasing differentiation commitment at the MPP cell level and self-renewal of HSCs.

### EP triggers a molecular response distinct from TPO-R signaling in HSCs

To investigate whether EP exerts its stem cell stimulatory effect through TPO-R activation, we determined and compared the molecular effects elicited by EP and rhTPO. We performed transcriptomic profiling of ex vivo-treated HSCs, which identified a total of 253 and 198 DEGs (compared to mock-treated controls) in rhTPO- and EP-treated stem cells, respectively (Fig. 2, A and B). rhTPO treatment resulted in the down- and up-regulation of 66 and 187 genes, respectively, whereas EP caused down- and up-regulation of 92 and 106 genes, respectively (Fig. 2, A and B and tables S1, S2). Supervised hierarchical clustering showed distinct gene expression profiles in rhTPO- and

**Fig. 2. EP triggers molecular pathways in human HSCs distinct from TPO signaling.** (A and B) Volcano plots showing the distribution of gene expression changes in human HSCs upon treatment with TPO (A) and EP (B). Up-regulated genes are indicated in red, whereas down-regulated genes are shown in green. (C) Supervised hierarchical clustering of expression profiles of HSCs treated with TPO, EP, or vehicle control (NT) using the genes differentially expressed among groups. (D) Venn diagram comparing DEGs between TPO- and EP-treated HSCs. (E) Enrichment analysis of DEGs containing iron-responsive elements (IREs) in TPO- or EP-treated HSCs. Hypergeometric test was used to calculate the significance ( $P$  value) of IRE enrichment. (F and G) Ingenuity pathway analysis (IPA) of upstream regulators (F) and canonical pathways (G) for DEGs specific to EP-treated HSCs. Top 10 pathways with significance  $P < 0.05$  are shown. The yellow and blue bars represent positive and negative Z scores, respectively. Black bars represent the  $-\log_{10}$  of the significance ( $P$  value). The red line represents the cutoff of significance ( $P = 0.05$ ). Iron-related pathways are shown in bold. (H) Quantitative real-time polymerase chain reaction (qRT-PCR) validation of DEGs in EP-treated HSCs. Fold changes of *HIF1A*, *HMOX1*, and *GADD45B* mRNA expression are shown. If not specified otherwise, then data are means  $\pm$  SEM. \* $P < 0.05$ , \*\* $P < 0.01$  (paired Student's  $t$  test).



Downloaded from <https://www.science.org> on August 15, 2023

EP-treated stem cells (Fig. 2C). Direct comparison of DEGs in the two treatment groups revealed only 40 genes with identical changes upon EP and rhTPO exposure, whereas 80% of the DEGs were specifically altered with one of the treatments (Fig. 2D and table S3), strongly suggesting that EP triggered molecular changes in HSCs distinct from those initiated upon TPO-R activation.

We next tested whether the observed gene expression changes may be a consequence of intracellular iron chelation and reduced LIPs because EP is also a highly potent intracellular iron chelator (17, 18). Reduction of intracellular LIP results in the stabilization of iron regulatory proteins (IRP1/2), which bind to IREs of mRNAs encoding genes critical for restoring iron homeostasis. In turn, this rapidly alters mRNA stabilization and translation (19). We screened mRNA sequences of DEGs for the presence of IRE-like motifs and found a significant enrichment in the number of IRE-containing genes differentially expressed upon EP ( $P = 8.2 \times 10^{-06}$ ) but not rhTPO treatment (Fig. 2E). We then subjected the list of EP-specific DEGs to canonical pathway and upstream regulator analyses, which revealed a significant enrichment of iron-related pathways, including iron ( $P = 0.0058$ ) and heme degradation ( $P = 0.035$ ) (Fig. 2, F and G, and table S4). We validated expression changes of genes involved in iron homeostasis, which included increased expression of *TFRC* (1.53-fold,  $P < 0.05$ ) and *SLC11A2* (1.47-fold,  $P < 0.05$ ) and up-regulated expression of mitochondrial iron transporters *SLC25A28* (1.20-fold,  $P < 0.05$ ) and *SLC25A37* (1.53-fold,  $P < 0.05$ ). In contrast, *FTL* (−1.40-fold,  $P < 0.05$ ), encoding the ferritin light-chain (FTL) protein, and hepcidin-encoding gene *HAMP* (−2.68-fold,  $P < 0.05$ ), facilitating iron storage, were significantly reduced (fig. S3A). Upstream regulator analysis revealed activation of *N*-acetyl-L-cysteine, emodin, epigallocatechin gallate, and miR-155-5p-mediated pathways, as well as inhibition of hydrogen peroxide and Toll-like receptor 2 (TLR2)-associated gene expression signatures (Fig. 2F). We furthermore detected reduced *HIF1A* mRNA and increased hypoxia-inducible factor 1 $\alpha$  (HIF1 $\alpha$ ) target gene expression, including up-regulation of genes with crucial roles in glycolysis (*HK1*, *PFKL*, and *PCK1*; Fig. 2H and fig. S3B), as well as evidence for CCAAT enhancer binding protein  $\alpha$  (CEBP $\alpha$ ) repression ( $Z$  score = −2.14;  $P = 0.048$ ; Fig. 2F). Alterations in genes associated with triacylglycerol biosynthesis and glycine degradation (Fig. 2G) further indicated metabolic reprogramming of EP-treated cells, consistent with an increased utilization of fatty acids and amino acids for energy production. These results show that EP elicits gene expression alterations in HSCs consistent with a molecular response to reduced intracellular iron content, consisting of decreased glycolysis and enhanced lipid and protein catabolic pathway activation.

### EP stimulates mouse HSCs independently of the TPO-R

EP's ability to activate TPO-R signaling is restricted to human and certain primate cells; murine receptor signaling cannot be stimulated by the small molecule (12). We used mouse HSCs as a separation-of-function model to test whether EP can exert a stem cell stimulatory effect in a TPO-R-independent fashion. Serial colony-forming assays with highly enriched HSCs isolated from wild-type mice revealed that EP increased serial replating of stem cells compared to control-treated cells, albeit without increasing multilineage colony formation in the initial plating (fig. S4A). We confirmed this finding using stroma-free long-term culture initiating cell (LTC-IC) assays, which also showed a 1.5-fold increase in functional stem cells in EP-treated cultures, compared to control-treated specimens (fig. S4B). To exclude the possibility that EP undergoes TPO-R-mediated internalization into

cells, we next tested HSCs derived from TPO-R-deficient (*c-Mpl*<sup>−/−</sup>) mice (20). Consistent with a previous report (21), we observed a significant ( $P < 0.0001$ ) reduction of phenotypic hematopoietic stem and progenitor cells, which was most pronounced at the level of stem cells in *c-Mpl*<sup>−/−</sup> compared to wild-type mice (fig. S5). Strikingly, upon *ex vivo* treatment of TPO-R-deficient cells, we found a significant increase in the serial replating capacity (1.6- to 2.2-fold,  $P < 0.05$ ) and LTC-IC frequency (1.8-fold,  $P = 0.04$ ), compared to control-treated cells (Fig. 3, A and B). We next quantified the number of functional HSCs upon *in vivo* treatment with EP (Fig. 3C). Daily oral gavage of TPO-R-deficient mice with EP resulted in clinically relevant EP plasma concentrations in mice (table S5) and a moderate but statistically significant increase (1.37-fold,  $P < 0.05$ ) in the number of phenotypical Lin<sup>−</sup>Sca<sup>+</sup>c-Kit<sup>+</sup>CD150<sup>+</sup>CD48<sup>−</sup> HSCs (Fig. 3D). LTC-IC assays furthermore revealed a significant increase (1.53-fold,  $P = 0.007$ ) of functional HSCs, compared to vehicle-treated control mice (Fig. 3, E and F). Limiting dilution bone marrow transplantation (BMT), routinely used for assessing stem cell frequency and function *in vivo* (22), showed a significant increase (1.6-fold,  $P = 0.03$ ) of stem cells derived from EP-treated donors, compared to control-treated donor mice (Fig. 3G). Despite the detectable increase in HSCs, *in vivo* treatment of TPO-R-deficient mice did not increase the numbers of mature erythroid, myeloid, or lymphoid cells (fig. S6), which were indistinguishable from wild-type mice (20); we also did not find an increase in platelets, owing to EP's inability to stimulate murine TPO-R signaling (fig. S6). Together, these findings demonstrate that EP can increase the number of functional HSCs independently of the TPO-R.

### EP activates iron homeostasis-restoring pathways in HSCs

As observed in human stem cells (Fig. 2), gene expression analysis of primary mouse HSCs and metabolic profiling of a mouse HSPC-like cell line (HPC7) (23) revealed molecular alterations consistent with the reduction of LIPs. Specifically, we identified a total of 232 DEGs in EP-treated HSCs compared to vehicle-treated control stem cells, with 113 up-regulated and 119 down-regulated genes (Fig. 4A and table S6). IRE motif prediction showed a significant enrichment of differentially expressed IRE-containing genes in EP-treated HSCs ( $P = 6.84 \times 10^{-11}$ ; Fig. 4B). Upstream regulator analysis furthermore revealed significant changes in the activity of a group of transcriptional regulators requiring iron as a cofactor [ $P = 0.0016$ , including *Slc40a1* (−1.50-fold), *Pcsk7* (−1.67-fold), *Slc11a2* (1.50-fold), and *Tnf* (1.51-fold); tables S6 and S7], as well as other factors affected by iron availability, such as hepcidin antimicrobial peptide (HAMP)/hepcidin ( $P = 8.10 \times 10^{-06}$ ), plasminogen (PLG) ( $P = 0.0015$ ), and RAB7B ( $P = 0.0013$ ; Fig. 4C and table S7). In addition, genes crucial for iron homeostasis, including *Tfrc* (encoding the transferrin receptor; CD71, increased by 2.6-fold) or *Ftl1*, *Slc40a1* [ferroportin (FPN)], *Hamp*, and *Hif1a* (by −1.27-fold, −1.50-fold, −3.99-fold, and −1.41-fold, respectively), were differentially expressed after EP treatment (Fig. 4D). Furthermore, we detected significantly increased CD71/TFRC surface protein abundance in primary HSCs ( $P < 0.05$ ) and a mouse hematopoietic stem and progenitor cell line, HPC7 ( $P < 0.01$ ), after EP treatment (Fig. 4, E and F). Quantification of free intracellular iron by FACS analysis using an iron-dependent fluorescent biosensor showed a significantly ( $P < 0.01$ ) reduced LIP size (as evidenced by an increased calcein fluorescence intensity upon LIP reduction) in EP-treated stem cells compared to control-treated primary HSCs (Fig. 4G). Pathway analysis of DEGs upon EP exposure revealed a significant enrichment

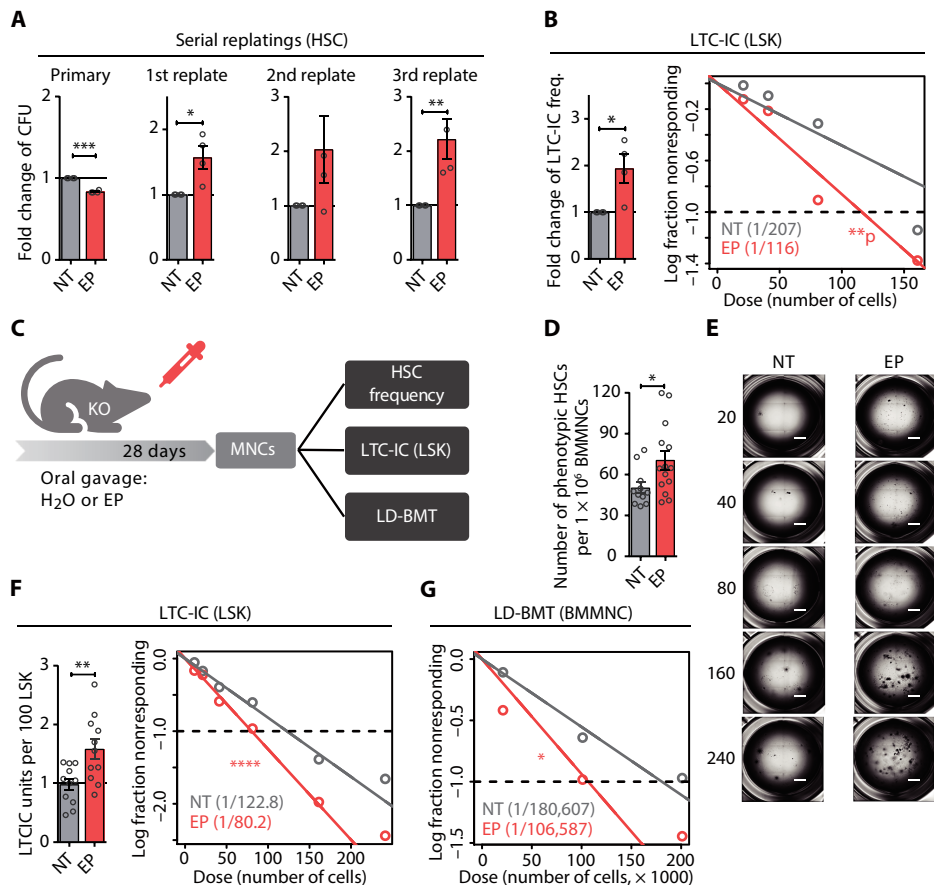


**Fig. 3. EP increases HSC self-renewal independently of the TPO-R.** (A) Serial colony-forming capacity of *Mpl*<sup>-/-</sup> HSCs treated with EP (10 μg/ml) compared to NT (water; *n* = 4). (B) LTC-IC assay of *Mpl*<sup>-/-</sup> Lin<sup>-</sup>Sca-1<sup>+</sup>c-Kit<sup>+</sup> (LSK) cells after ex vivo treatment with vehicle control (NT) or EP. Left: Bar plot showing the fold change of LTC-IC frequency compared to NT, estimated for each of the individual mice (*n* = 4, paired *t* test). Right: Scatter plot showing LTC-IC frequency for EP and NT. (C) Scheme showing in vivo treatment schedule of *Mpl*<sup>-/-</sup> mice. Mice were treated with EP daily for 28 days, followed by immunophenotypic and functional assessment of HSC frequency. KO, knockout. (D) Frequency of phenotypic HSCs within the bone marrow after EP (*n* = 14 mice) or vehicle treatment (NT; *n* = 12 mice). \**P* < 0.05 (unpaired *t* test). (E and F) Representative images (E) and fold change of stem cell frequency (F) assessed by LTC-IC assay for *Mpl*<sup>-/-</sup> LSK cells. Scale bars, 1 mm. (G) HSC frequency in EP-treated mice compared to control determined by limiting dilution transplantation. Results are pooled from five independent experiments (*n* = 74 and 70 recipient mice for NT and EP, respectively). If not specified otherwise, then data are means ± SEM. \**P* < 0.05, \*\**P* < 0.01, \*\*\**P* < 0.001, \*\*\*\**P* < 0.0001 (paired Student's *t* test).

in factors associated with iron and oxygen homeostasis, including glutathione redox reactions (*P* = 0.02) and glutathione-mediated detoxification (*P* = 0.03) pathways (Fig. 4H), which are consistent with reduced reactive oxygen species (ROS) concentrations and HIF1α activation, commonly observed after iron chelator treatment (18, 24–29). We further found DEGs enriched for PXR/RXR activation, sucrose degradation, and galactose degradation (Fig. 4H) and observed up-regulation of glycolytic genes (*Pfkf*, *Mxi1*, and *Pgm1*; fig. S7). Metabolite analysis of EP-treated HPC7 cells confirmed significantly (*P* < 0.001) enhanced galactose metabolism and pantothenate and CoA biosynthesis (Fig. 4I and tables S8 and S9), as well as alterations in glycolysis (*P* = 4.1 × 10<sup>-6</sup>; Fig. 4J and table S10). We detected increased concentrations of glucose-6-phosphate (G6P), mannose, glycerol, glucose, and citric acid (intermediates of glycolytic pathways), as well as impaired aminoacyl-transfer RNA (tRNA) biosynthesis (Fig. 4I and

table S9) in cells treated with EP, suggesting impairment of iron-dependent nonenzymatic isomerization and tRNA ligation reactions in EP-treated cells. As in human EP-treated stem cells, we found evidence for increased mobilization of fatty acids and a reduction of several amino acids (lysine, tyrosine, isoleucine, proline, cysteine, glycine, glutamate, and valine), which can enter glycolytic pathways (Fig. 4, H and I). Together, these observations show that EP elicits a molecular response consistent with lower intracellular iron pools, including iron homeostasis-restoring gene expression alterations, as well as metabolic alterations due to reduced iron and ROS concentrations.

### Iron chelation critically contributes to the stem cell stimulatory effect of EP

To functionally assess whether the iron-chelating property of EP mediated its stem cell stimulatory effect, we applied a two-pronged strategy using mouse HSCs: (i) We subjected primary stem cells to a 1-hour pretreatment with ferric ammonium citrate (FAC) at a concentration that does not impair stem cell function (fig. S8A), does not exceed the chelating capacity of EP (fig. S8, B and C), and does not increase ROS in EP-treated stem cells (fig. S9); and (ii) we tested two additional clinically available iron chelators, deferoxamine (DFO) and deferasirox (DFX). Our data show that DFO and DFX increased ex vivo HSC self-renewal, just as EP did, and that iron preloading prevented this effect for all three chelators tested (fig. S10).

We next tested whether iron chelator treatment would also increase human HSC function. Exposure of human CD34<sup>+</sup> stem and progenitor cells to DFO, DFX, or EP consistently increased ex vivo self-renewal of human stem cells (Fig. 5, A to D), whereas iron preloading prevented this effect (Fig. 5, C and D). These findings demonstrate that the reduction of intracellular LIPs upon EP, DFO, or DFX treatment can increase ex vivo self-renewal of human HSCs.

Last, we assessed human HSC function upon in vivo treatment with EP. qRT-PCR on bone marrow mononuclear cells (BMMNCs) from patients with ITP under EP therapy (see table S11 for detailed patient information) uncovered gene expression alterations consistent with iron homeostasis-restoring pathway activation compared to control stem cells. We specifically found reduced expression of iron storage protein-encoding *FTL* (−1.86-fold, *P* < 0.05), master regulator of iron homeostasis-encoding *HAMP* (2.4-fold, *P* < 0.05), and significantly increased transcription of genes encoding iron transporters *TFRC*, *SLC11A2*, *SLC25A28*, and *SLC25A37* (by 9.1-, 2.1-, 1.8-, and 1.7-fold, respectively) (*P* < 0.05; fig. S11A). To exclude the possibility that the observed gene expression alterations in EP-treated patients were due to preexisting aberrant iron profiles, we analyzed

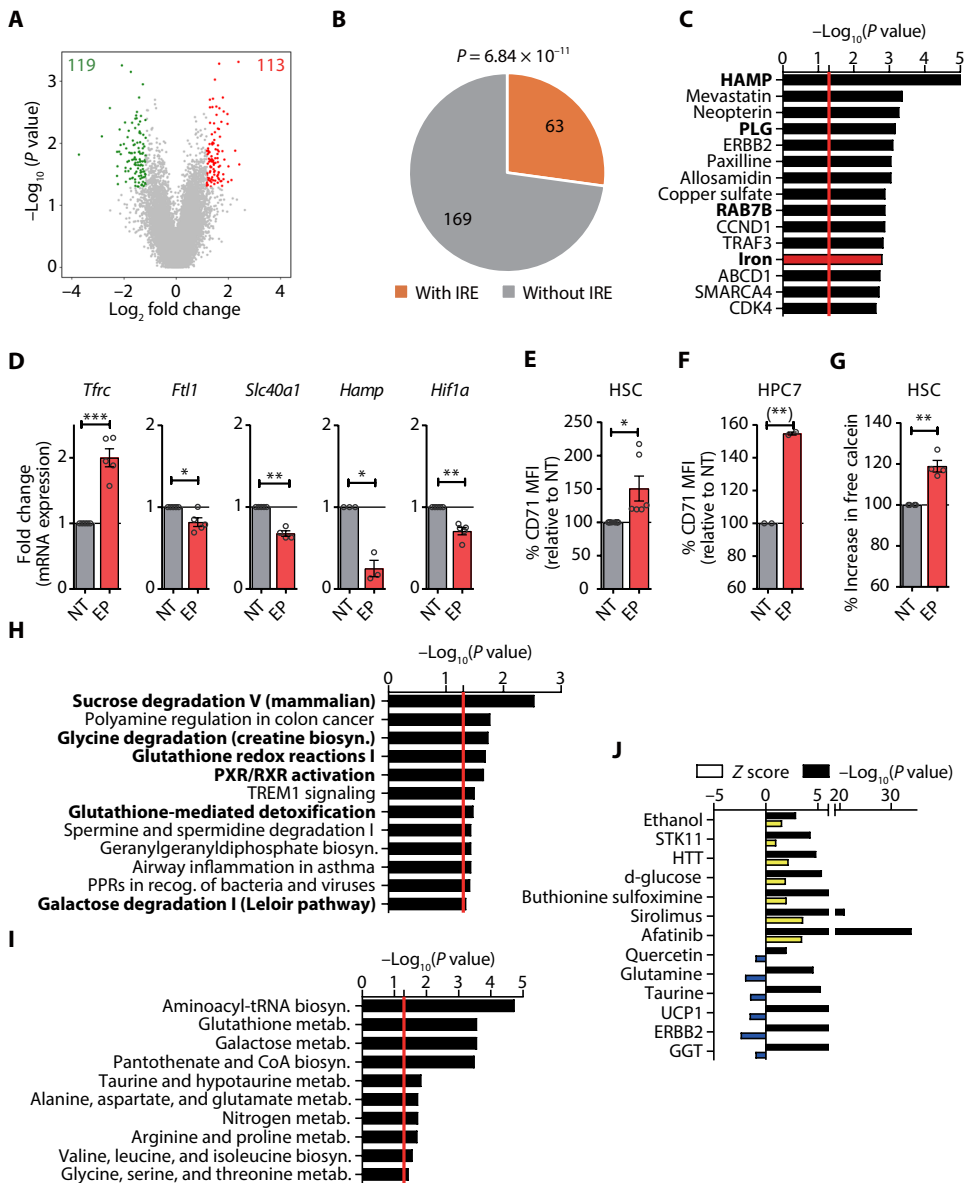


**Fig. 4. EP induces molecular changes consistent with intracellular iron reduction.** (A) Distribution of expression changes in HSCs upon EP treatment. (B) Enrichment analysis of DEGs containing IREs in EP-treated HSCs. (C) IPA analysis of upstream regulators of DEGs. (D) Fold change of *Tfr*, *Ftl*, *Slc40a1*, *Hamp*, and *Hif1a* in EP-treated HSCs by qPCR. (E and F) Change of CD71/TFRC mean fluorescence intensity (MFI) in HSCs (E) or HPC7 cell line (F) after EP treatment [ $n = 6$  and  $2$ , respectively, for (E) and (F)]. (G) Calcein staining to measure the concentration of intracellular iron. Results are presented as MFI of calcein in HSCs treated with EP relative to NT. (H) IPA of canonical pathways with DEGs in EP-treated HSCs. Top 10 pathways with significance of  $P < 0.05$  are shown. (I and J) IPA of canonical pathways (I) and upstream regulators (J) with altered metabolites (fold change  $> 1.5$  or  $< -1.5$ ) in the metabolite profiling of HPC7 cells with EP treatment ( $n = 4$ ). The yellow and blue bars represent positive and negative Z scores, respectively. Black bars represent the  $-\log_{10}$  of the significance ( $P$  value). The red line represents the cutoff of significance ( $P = 0.05$ ). If not specified otherwise, then data are means  $\pm$  SEM. \* $P < 0.05$ , \*\* $P < 0.01$ , \*\*\* $P < 0.001$  (paired Student's  $t$  test).

expression of iron-responsive mRNAs using published data sets from hematopoietic stem and progenitor cells derived from patients with acute or chronic ITP who had not received EP treatment (30, 31). This analysis revealed no significant changes in any known iron-responsive transcripts, except for *FTL*, which was moderately increased in patients with chronic ITP (fig. S11, B and C).

We next determined and compared the functional effects of EP and romiplostim, another U.S. Food and Drug Administration-approved TPO-RA, which does not harbor an iron-chelating ability, on human HSCs. FACS analysis of bone marrow specimens (table S11) to quantitate the number of phenotypic stem cells revealed a three-fold increase in the frequency of phenotypic HSCs ( $\text{Lin}^- \text{CD34}^+ \text{CD38}^- \text{CD49f}^+$ ) in patients treated with EP, compared to romiplostim-treated individuals (Fig. 5, E to G), suggesting a stem cell stimulatory effect in vivo. We quantified the number of functional HSCs in the bone marrow of patients undergoing TPO-RA therapy, which confirmed the significant increase in the number of functional stem cells (by threefold,  $P < 0.001$ ) in samples derived from EP-treated patients compared to romiplostim-treated controls (Fig. 5, H and I). Together, these results provide evidence for iron chelation as a mechanism underpinning EP-mediated stimulation of HSC self-renewal.

## DISCUSSION

Previous clinical and preclinical studies have provided evidence for the multilineage stimulation of hematopoiesis upon EP treatment, which suggested that the TPO-RA may directly stimulate immature hematopoietic stem and progenitor cells (15, 16, 32). Our results using highly enriched human bone marrow-derived HSCs (33) exposed to EP ex vivo show an increase in multilineage differentiation and the number of functional stem cells persisting upon long-term culture. Moreover, quantification of phenotypic and functional stem cells in patients undergoing EP therapy also showed a moderate increase in the number of stem cells, which demonstrates that enhanced multilineage hematopoiesis observed in patients upon EP treatment (15, 16, 32) is, at least in part, attributable to a direct stimulation of stem cells.

Our comparative analysis of the stem cell-specific effects of EP and romiplostim, another clinically approved TPO-RA without metal ion-chelating characteristics, revealed a stronger stimulation of HSCs by EP. This functional difference does not appear to solely stem from enhanced TPO-R stimulation by EP due to its noncompetitive binding of the cytokine receptor (17, 34) because we did not find evidence for enhanced TPO-R activation at the molecular level in EP-treated stem cells. Moreover, wild-type and *c-Mpl*-deficient mouse HSCs, in which TPO-R signaling cannot be

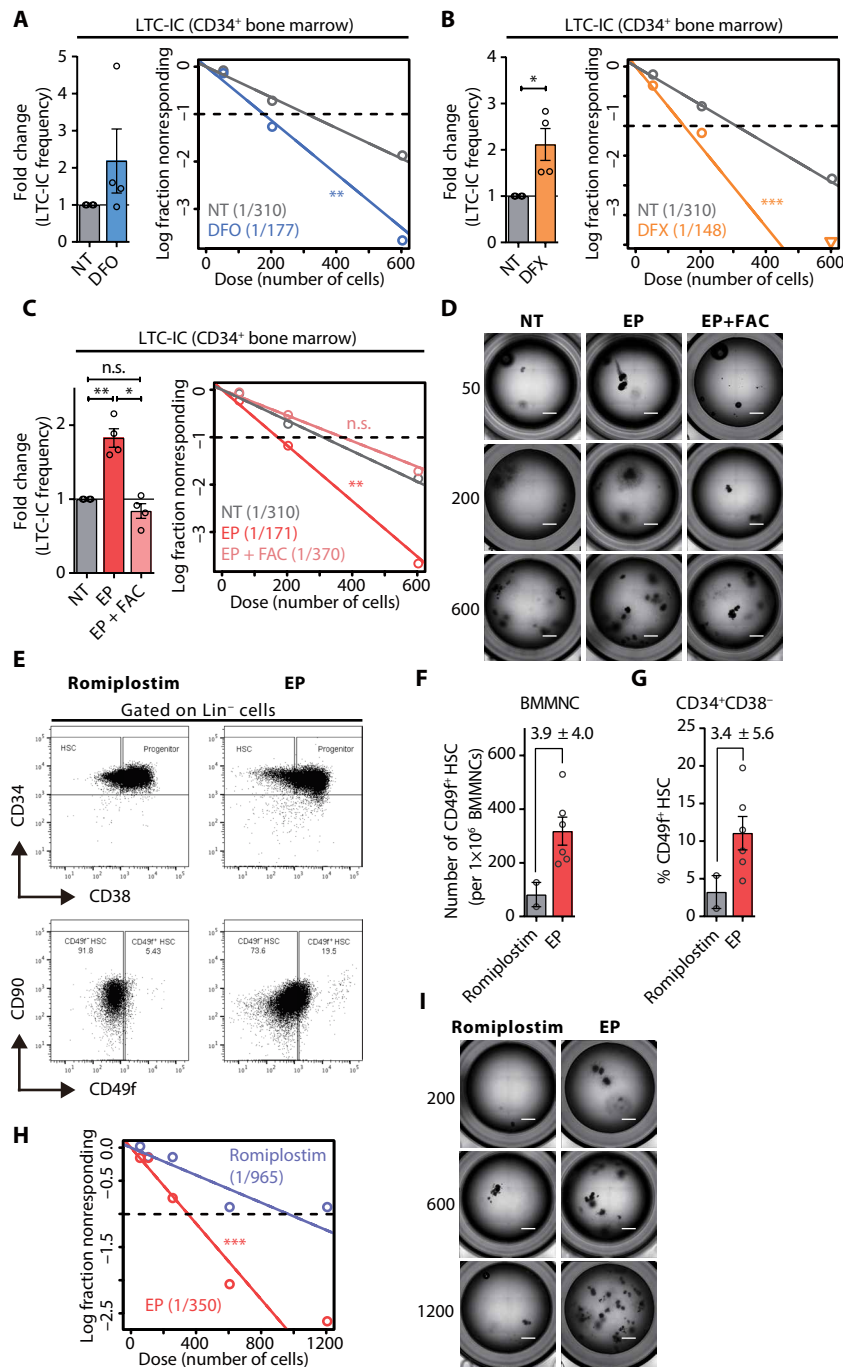


**Fig. 5. EP increases the number of functional long-term HSCs in patients with hematopoietic deficiency.** (A to C) HSC frequency in healthy donors enumerated by the LTC-IC assay. Left: LTC-IC frequency in each individual donor ( $n = 4$ ). Right: Scatter plot showing LTC-IC frequency of CD34<sup>+</sup> cells in NT versus those treated with iron chelators DFO (10  $\mu$ M) (A), DFX (5  $\mu$ M) (B), or EP with or without rescue (C). n.s., not significant. (D) Representative images of LTC-IC assay showing limiting dilutions of CD34<sup>+</sup> cells from healthy donors treated ex vivo with either vehicle (NT) or EP with or without rescue (EP + FAC). (E) FACS analysis of HSCs (Lin<sup>-</sup>CD34<sup>+</sup>CD38<sup>-</sup>CD49f<sup>+</sup>) in ITP patients treated with either romiplostim (control) or EP. (F and G) Quantification of phenotypic HSCs within BMMNC (F) and CD34<sup>+</sup>CD38<sup>-</sup> (G) compartments. (H) Representative images of LTC-IC assay showing CD34<sup>+</sup> cells from ITP patients treated in vivo with romiplostim (control) or EP. (I) HSC frequency in ITP patients treated in vivo with romiplostim ( $n = 2$ ) or EP ( $n = 4$ ). Scale bars, 1 mm. LTC-IC assay. HSC frequencies were estimated by Poisson statistics using extreme limiting dilution analysis (ELDA). If not specified otherwise, then data are means  $\pm$  SEM. \* $P < 0.05$ , \*\* $P < 0.01$ , \*\*\* $P < 0.001$  (paired Student's  $t$  test).

activated by EP (12), showed increased stem cell maintenance and self-renewal upon treatment with EP. Iron preloading eliminated this effect, which provided further evidence that EP's stem cell stimulatory effect is largely exerted by chelation of intracellular iron. Whether and how TPO-R activation or chelation of bivalent cations other than iron, such as Ca<sup>2+</sup> (35, 36), contributes to EP's functional effects in enhancing multilineage hematopoiesis could be addressed in future studies. Together, our data suggest an additive effect of the TPO-R-stimulatory and iron-chelating effects of EP in enhancing HSC function in humans, which would be interesting to further dissect mechanistically in future studies.

Iron is an essential element facilitating catalysis of enzymatic reactions that involve electron transfer (37). Various proteins containing iron-sulfur clusters (Fe-S) or heme groups depend on iron as a cofactor (38, 39). The most readily chelatable form of iron within cells is termed the LIP and comprises both Fe<sup>2+</sup> and Fe<sup>3+</sup>; its size is determined by a cell's particular need for readily accessible iron and is kept at the minimally required concentration at any given moment due to its ability to generate ROS via the Fenton reaction (40). Preclinical studies revealed that EP is highly cell-permeable and reduces free intracellular iron by acting as a shuttle chelator with a high binding affinity for Fe<sup>3+</sup>, reducing intracellular ROS accumulation and effective intracellular iron storage mobilization in several different cell types (18, 24).

Two large clinical studies with non-iron-overloaded patients reported moderately reduced serum transferrin and ferritin concentrations (41, 42), but chronically reduced iron concentrations, iron deficiency, or changes in erythropoiesis have not been observed (43, 44). These clinical findings show that EP can curtail free extra- and intracellular iron pools in patients, which appears to elicit a compensatory response of iron mobilization and reinstatement of iron homeostasis during EP treatment. In line with these observations, our molecular profiling of human and mouse HSCs revealed gene expression and metabolic alterations similar to those found with acutely reduced intracellular iron concentrations, including altered gene expression, reduced ROS accumulation, and metabolic adaptations. We found compensatory increase of factors facilitating iron intake, including *TFR/CD71* (transferrin receptor), *SLC11A2* (encoding DMT1), *SLC25A28*, and *SLC25A37* (19, 45) upon EP exposure of HSCs. Concomitantly, genes enhancing iron storage and export, including *FTL*, *HAMP/hepcidin*, and *FPN* (46), were reduced upon EP exposure. Pathway analysis furthermore revealed gene expression changes similar to those found upon impairment of nitric oxide (NO) and TLR2 signaling, which also cause the activation of IRP1 (47, 48). IRP1 is a bifunctional protein that, under iron-replete conditions, displays an [4Fe-4S] cluster at the active

site and harbors aconitase activity (49). At low intracellular iron concentrations, IRP1 binds IREs located in untranslated regions (UTRs) of mRNAs and alters their stability and translation (19). For those transcripts with IRE motifs present on the 3' UTR, such as *TFRC* and *SCL11A2*, IRP binding stabilizes the mRNA, resulting in increased transcription compared to iron-replete conditions. In line with this known regulatory mechanism is the increased expression of *TFRC* and *SCL11A2* upon EP treatment. For transcripts with the IRE motifs located in the 5' UTR, such as *FTH1*, *FTL*, and *SLC40A1* (*FPN*), IRP binding blocks the translation of the transcript, resulting in a decrease in protein in the presence of unaltered transcript amounts (50). Notably, we found reduced amounts of *FTL* and *SLC40A1* transcripts in EP-treated HSCs, suggesting a negative feedback loop at the transcriptional level. Moreover, we found gene expression changes consistent with increased miR155-5 expression and reduced dopamine and heme oxygenase 1 (HMOX-1) concentrations, which have been reported in iron-deficient cells (51–53). In line with previous reports demonstrating that EP efficiently reduces ROS (18, 24, 54, 55), likely due to lower Fenton reaction rates upon the reduction of cheatable iron species (56), we found reduced ROS, hydrogen peroxide, and GADD45B signaling (24), as well as molecular alterations mimicking known antioxidants (57). Reduction of free intracellular iron also impairs the activity of prolyl hydroxylase domain (PHD) enzyme, resulting in the stabilization of HIF1 $\alpha$  under normoxic conditions (29), which can enhance HSC maintenance and function (58). EP-mediated gene expression changes are also in agreement with this finding because we detected reduced *HIF1A* mRNA and impaired CEB- $\beta$ -driven gene expression, which have been shown to be negatively regulated by HIF1 $\alpha$  (59). HIF1 $\alpha$  can also impair *Hamp* expression in hepatocytes during anemia and hypoxia (28); our data on reduced *Hamp* expression after EP treatment suggest the activation of a similar direct gene regulatory circuit in stem cells upon LIP reduction.

EP also elicited several metabolic alterations in HSCs upon acute exposure, including iron-catalyzed nonenzymatic metabolic reactions (60–62), which can occur alongside enzymatic reactions between glycolytic intermediates (63), as evidenced by our finding of high concentrations of D-glucose, G6P, and D-mannose upon EP treatment. The accumulation of G6P and impairment of aminoacyl-tRNA biosynthesis upon EP exposure further agrees with impaired nonenzymatic PPP and RNA biosynthesis (64, 65). Our data moreover suggest that impairment of nonenzymatic reactions results in inefficient glycolysis and PPP, which elicits compensatory reactions to meet the cells' energetic requirements, namely, increased galactose degradation through the Leloir pathway (66), increased lipolysis mobilizing triglycerides that can enter glycolytic pathways through  $\beta$ -oxidation (67), and an increased use of amino acids for energy production. Increased concentrations of citric acid found in EP-treated cells further suggest increased tricarboxylic acid cycle activity. Metabolic reprogramming upon EP treatment also included several pathways that enhance HSC maintenance and function, such as activation of STK11/LKB1 (68–70), suppression of mammalian target of rapamycin (mTOR) activity, and the reduction of fumarate concentrations (71, 72).

Together, our data demonstrate a TPO-R-independent stem cell stimulatory function of EP and suggest that free intracellular iron pools may serve as a rheostat for HSC maintenance. The iron chelation-dependent mechanism of EP is very likely to confer clinical relevance in the context of enhancing TPO-R-dependent HSC stimulation and reinforcing stem cell identity through wide-ranging iron-dependent metabolic reprogramming, which increases healthy stem cells without

causing their exhaustion in bone marrow failure syndromes, as well as aid in preserving functional HSCs under cellular stress (such as transplantation, cytotoxic treatment, or irradiation). Future studies will be needed to dissect how alterations in LIP size inform stem cell identity upon cell division and how pathologically increased or decreased systemic iron triggers molecular and functional alterations of hematopoietic and potentially other tissue-specific stem cells.

## MATERIALS AND METHODS

### Study design

The purpose of the study was to define the molecular and cell functional mechanism of action of EP. Stem cell self-renewal and differentiation commitment of primary cells isolated from human or mouse bone marrow were assessed in vitro using LTC-IC and serial colony assays in the presence of EP (3 to 10  $\mu$ g/ml) or 10 and 5  $\mu$ M DFO and DFX, respectively. FAC (200  $\mu$ g/ml) was used in rescue experiments after dose-finding experiments, which determined the maximal dosage of FAC that did not change ex vivo HSC function. Cells were either treated throughout the duration of the assay or pretreated for over 2 days. End points measuring ex vivo self-renewal and differentiation commitment were chosen on the basis of previously determined timelines. All cellular experiments were conducted using three or more biological replicates, which were measured in at least technical duplicates. All experiments were performed unblinded with at least two independent repeats. In vivo studies to determine the effects of EP treatment on mouse stem cell function consisted of the treatment of 8- to 12-week-old wild-type or *c-Mpl*<sup>-/-</sup> mice with EP (50 mg/kg) or vehicle (water) by daily oral gavage for 28 days. Accumulation of EP in the serum of treated mice was confirmed. Limiting BMTs of EP-treated donor mice were used to quantify the number of functional stem cells in vivo. Age-matched recipient and donor mice of both genders were included in these studies. The end point of these studies was 16 weeks after transplantation, a previously determined time frame allowing the assessment of stem cell function. Exclusion criteria included unspecified death of animals or loss of more than 20% of body weight. These experiments were carried out in an unblinded fashion using at least three biological replicates and measured in at least technical triplicates. Experiments were carried out in at least two independent repeats.

### Patient samples and cell lines

Healthy cryopreserved human bone marrow cells were purchased from AllCells and ReachBio Research Labs; fresh unprocessed bone marrow cells were from Lonza. Samples of patients with ITP are listed in table S11. HPC7 cells were obtained from O. Abdel-Wahab at the Memorial Sloan Kettering Cancer Center and grown in Iscove's Modified Dulbecco's Medium (IMDM) supplemented with recombinant mouse stem cell factor (rmSCF) (100 ng/ml; Gemini Bio-Products), monothio-glycerol (6.9 ng/ml; Sigma-Aldrich), 5% fetal bovine serum (FBS), 1% sodium pyruvate, and 1% penicillin/streptomycin. All experiments were approved by the Institutional Review Board of the Albert Einstein College of Medicine (protocol nos. 2016-6770 and 2016-1003).

### Cell preparation and purification of human hematopoietic stem and progenitor cells

The bone marrow was enriched for mononuclear cells by density gradient centrifugation using Ficoll-Paque PLUS (GE Healthcare). Mononuclear cells were further enriched for CD34<sup>+</sup> cells by immunomagnetic



bead sorting (CD34 MicroBead Kit, human; Miltenyi Biotec) according to the manufacturer's protocol. CD34<sup>+</sup> cells then underwent two sequential incubations with antibodies against surface markers defining lineage-positive cells, progenitors, and HSCs. The primary antibody cocktail contained CD2, CD3, CD4, CD7, CD8, CD10, CD11b, CD14, CD19, CD20, CD56, CD235A, and CD90/Thy1, and the secondary antibody cocktail contained CD34, CD38, and CD49f. A list of antibodies can be found in table S12. Antibody staining was performed at 4°C in the dark for 30 min. Cells were washed with phosphate-buffered saline (PBS)/2% bovine serum albumin/2 mM EDTA between stains. Cells were sorted on FACS Aria II (Becton Dickinson) with a 100- $\mu$ m nozzle operating in purity mode and collected in 1.5-ml microfuge tubes containing IMDM/2%FBS. FACS data were analyzed using FlowJo version 10.2.

### Purification of mouse hematopoietic stem and progenitor cells

*c-Mpl*<sup>-/-</sup> mice were provided by W. Tong (University of Pennsylvania). C57BL/6J and B6.SJL-Ptprc<sup>a</sup> Pepc/BoyJ mice were purchased from the Jackson Laboratory. All mice were housed in a specific pathogen-free barrier facility. All experimental procedures conducted on mice were approved by the Institutional Animal Care and Use Committee of the Albert Einstein College of Medicine (protocol no. 2016-0103). For FACS experiments, bone marrow cells were isolated from tibiae, femurs, pelvic bones, and vertebrae of 6- to 10-week-old mice by gentle crushing with a mortar and pestle in sterile PBS (Gibco). Low-density mononuclear cells were enriched by density gradient centrifugation using Histopaque 1083 (Sigma-Aldrich), followed by staining of lineage (CD3, CD4, CD8a, CD19, B220, Ter119, and Gr1; 1:100) and stem and progenitor cell markers (Sca-1, c-Kit, CD150, CD48, and CD34; 1:50). A detailed list of antibodies can be found in table S12. Prospective HSCs (Lin<sup>-</sup>Sca-1<sup>+</sup>c-Kit<sup>+</sup>CD150<sup>+</sup>CD48<sup>-</sup>CD34<sup>-</sup>), MPPs (Lin<sup>-</sup>Sca-1<sup>+</sup>c-Kit<sup>+</sup>CD150<sup>-</sup>CD48<sup>-</sup>), and progenitors (Lin<sup>-</sup>Sca-1<sup>+</sup>c-Kit<sup>+</sup>CD150<sup>-</sup>CD48<sup>+</sup>) were sorted on either FACS Aria II (Becton Dickinson) or MoFlo Astrios (Beckman Coulter) with a 70- $\mu$ m nozzle operating in purity mode and collected in 1.5-ml microfuge tubes containing IMDM/2% FBS. Cells were sorted according to the gating strategy shown in fig. S5.

### Colony formation and serial replating assays

Human HSCs (Lin<sup>-</sup>CD34<sup>+</sup>CD38<sup>-</sup>CD49f<sup>+</sup>) and MPPs (Lin<sup>-</sup>CD34<sup>+</sup>CD38<sup>-</sup>CD49f<sup>-</sup>) were FACS-sorted and cultured in rhTPO-free MegaCult-C medium (STEMCELL Technologies) to assess colony formation of MK progenitors, according to the manufacturer's instructions. Colonies were scored after 10 to 12 days using an Inverted Infinity and Phase Contrast Microscope (Fisher Scientific). To assess the colony formation of myeloid and erythroid progenitors, stem and progenitor cells were plated in HSC003 (human) or HSC007 (mouse) methylcellulose medium according to the manufacturer's recommendation (R&D Systems). Colonies were scored after 14 to 16 days for human and 8 to 12 days for mouse using an Inverted Infinity and Phase Contrast Microscope (Fisher Scientific). In the serial replating assay, methylcellulose medium from primary plating was dissolved in PBS to dissociate the colonies into a single-cell suspension. Subsequently, 20,000 cells from the previous plating were serially replated in 1 ml of HSC003 or HSC007 medium for human and mouse cells, respectively.

### Single cell division assay of human HSCs

Single human HSCs (Lin<sup>-</sup>CD34<sup>+</sup>CD38<sup>-</sup>CD49f<sup>+</sup>) were sorted with FACS Aria II (Becton Dickinson) and directly deposited onto a 60-well

Terasaki plate (Thermo Fisher Scientific). Sorted cells were cultured in MyeloCult H5100 medium (STEMCELL Technologies) supplemented with recombinant human stem cell factor (rhSCF) (100 ng/ml; Gemini Bio-Products) and 10<sup>-6</sup> M hydrocortisone (Acros Organics) supporting stem cell maintenance, along with treatment with vehicle control (sterile H<sub>2</sub>O), EP (3 or 10  $\mu$ g/ml; Novartis), or rhTPO (100 ng/ml; Gemini Bio-Products). Single-cell deposition in each well was verified 4 hours after seeding, and cells per well were counted again at 24, 48, 72, 96, and 120 hours after treatment using an Inverted Infinity and Phase Contrast Microscope (Fisher Scientific).

### Cell cycle assays of human HSCs

Human HSCs (Lin<sup>-</sup>CD34<sup>+</sup>CD38<sup>-</sup>CD49f<sup>+</sup>) were sorted with MoFlo Astrios (Beckman Coulter) and cultured in MyeloCult H5100 medium (STEMCELL Technologies) supplemented with rhSCF (100 ng/ml; Gemini Bio-Products) along with treatment with vehicle control (sterile H<sub>2</sub>O), EP (3 or 10  $\mu$ g/ml; Novartis), or rhTPO (100 ng/ml; Gemini Bio-Products) for 24 hours. To assess cell cycle entry (G<sub>0</sub> to G<sub>1</sub> transition), the cells were subsequently washed with PBS and fixed with BD Cytotfix/Cytoperm (BD Biosciences) for 10 min at 4°C. After fixation, cells were washed twice with Perm/Wash (BD Biosciences), resuspended in 100  $\mu$ l of Perm/Wash containing anti-Ki-67 (BD Pharmingen), and incubated overnight at 4°C. Before analysis, cells were incubated with Hoechst 33342 (2  $\mu$ g/ml) for 10 min at 4°C.

To assess cell cycle status (G<sub>1</sub>, S, and G<sub>2</sub>/M), human HSCs were pulsed with 2  $\mu$ M 5-ethynyl-2'-deoxyuridine (EdU) for 6 hours, followed by fixation and EdU detection using the Click-iT EdU Flow Cytometry Kit (Invitrogen) following the manufacturer's recommendation. Before analysis, cells were incubated with propidium iodide (BD Biosciences) for 15 min at room temperature. Data were analyzed using FlowJo software version 10.2 (FlowJo LLC).

### RNA extraction, qPCR, and gene expression analysis by microarray

RNA was extracted using the RNeasy Micro Kit (QIAGEN), and its quantity and quality were assessed using NanoDrop 3300 Fluorospectrometer (Thermo Fisher Scientific) or Agilent 2100 Bioanalyzer (Agilent Technologies). For qPCR, reverse transcription of extracted RNA was performed using SuperScript II Reverse Transcriptase (Invitrogen), and qPCR was performed with PCR Power SYBR Green mix (Applied Biosystems) on a ViiA 7 Real-Time PCR system (Applied Biosystems) according to the manufacturer's instructions. mRNA signals were normalized to internal control *GAPDH* (glyceraldehyde-3-phosphate dehydrogenase), and a list of qPCR primers for target genes can be found in table S13. For microarray studies, extracted RNA was amplified and labeled using the GeneChip 3' IVT Pico Kit (Affymetrix). The products were then hybridized to GeneChip Human Gene ST 2.0 or Mouse Clariom S microarrays (Affymetrix) for human and mouse samples, respectively. Thereafter, hybridization signals were scanned and analyzed with a GeneChip Scanner 3000 7G system (Affymetrix) according to standard protocols.

### Analysis of microarray data

For analysis of microarray data, intensity normalization was performed across samples with the CEL files using RMA (robust multichip average) algorithm of an Oligo Bioconductor package (73). Normalized expression values were used as input for Qlucore version 3.2 (Qlucore AB). Multigroup comparison with *F* test resulted in 668 genes with *P* < 0.05, which were subsequently used for performing hierarchical

clustering based on Euclidean distances and average linkage to compare the expression profiles between TPO- or EP-treated human HSCs. For analysis of differential gene expression, a paired, linear modeling of limma Bioconductor package was used to compare the treated samples versus the matched, nontreated controls (74). Differential expression was defined as fold change > 1.5 (both up and down in TPO or EP compared to vehicle) and  $P < 0.05$  as estimated with limma. DEGs were subsequently subjected to IPA (QIAGEN) for analyses of canonical pathways and upstream regulators. For enrichment of IRE-containing genes, the National Center for Biotechnology Information RefSeq mRNA sequences of all the genes detected by the array platform were computationally screened for IRE-like motifs using SIREs Web server 2.0 (75, 76). Thereafter, hypergeometric test by built-in phyper function of R (www.R-project.org) was used to examine the significance of enrichment of IRE-containing genes within the DEGs in each treatment condition.

For the analysis of published gene expression data sets, GSE5812 was downloaded and normalized using Qlucore version 3.2 for comparing patients with acute ITP to healthy controls (30). Expression data of patients with chronic ITP were obtained from GSE23754 (31) and compared to those of healthy controls in GSE5812. Batch effects of the respective data sets were removed using the ComBat module of sva Bioconductor package (77, 78).

### Conditioned medium for LTC-IC assay

For collection of mouse stroma cell-conditioned medium, bone marrow cells were isolated from tibiae, femurs, pelvic bones, and vertebrae of 6- to 12-week-old mice by gentle crushing in sterile PBS. Total bone marrow cells were cultured overnight in Dulbecco's modified Eagle's medium (DMEM) supplemented with 10% FBS and 1% penicillin/streptomycin [penicillin (100 U/ml) and streptomycin (100 µg/ml); Mediatech Inc.]. Nonadherent cells were removed, and the remaining adherent cells were cultured until 80 to 90% confluency and subsequently irradiated (20 Gy) to suspend cell proliferation. Four to 5 hours after irradiation, adherent stromal cells were cultured in MyeloCult M5300 (STEMCELL Technologies) supplemented with Primocin (200 µg/ml; InvivoGen), and medium was collected, sterile-filtered every 48 hours, and then stored at  $-20^{\circ}\text{C}$  in aliquots until use.

For collection of human stroma cell-conditioned medium, HS-5 (CRL-11882, American Type Culture Collection) bone marrow stromal cells were cultured in DMEM supplemented with 10% FBS and 1% penicillin/streptomycin. Once at 80 to 90% confluency, cells were irradiated at 20 Gy and cultured in MyeloCult H5100 (STEMCELL Technologies) supplemented with Primocin (200 µg/ml; InvivoGen). Conditioned medium was collected, sterile-filtered every 48 hours, and then stored at  $-20^{\circ}\text{C}$  in aliquots until use.

### LTC-IC assay

To assess LTC-IC frequency in mouse, serial dilutions of FACS-sorted Lin<sup>-</sup>Sca-1<sup>+</sup>c-Kit<sup>+</sup> (LSK) cells were plated in MyeloCult M5300 (STEMCELL Technologies) mixed at 50:50 ratio with primary mouse stroma cell-conditioned medium as described above. To assess LTC-IC frequency in human, serial dilutions of mononuclear cells or immunomagnetically enriched CD34<sup>+</sup> cells were plated in MyeloCult H5100 (STEMCELL Technologies) mixed at 50:50 ratio with HS5-conditioned medium as described above. In each experiment, 10 technical replicates of each cell dose (indicated in the main text) were performed. After 4 weeks (mouse) or 5 weeks (human) of culture, each well was assayed in HSC007 and HSC003 (R&D Systems), respectively, in mouse and human, for the presence of CFU-C as described be-

fore (79). HSC frequency within the tested cell population was estimated using ELDA software (<http://bioinf.wehi.edu.au/software/elda/>) (80).

### Limiting dilution-competitive BMT assay

Frequency of HSCs was measured by limiting dilution-competitive BMT assay. Bone marrow cells of CD45.2 donor mice from each treatment group (vehicle control versus EP) were depleted of red blood cells by brief treatment with ammonium chloride potassium (ACK) buffer for 1 min on ice. The resulting BMMNCs were serially diluted into 20,000, 100,000, and 200,000 cell dose fractions. To prepare Sca-1-depleted helper cells, ACK-lysed bone marrow cells from CD45.1 Pepc/BoyJ mice were incubated with biotinylated Sca-1 antibodies in  $4^{\circ}\text{C}$  for 30 min, followed by binding to magnetic beads (Dynabeads Untouched Mouse T Cells Kit, Thermo Fisher Scientific) at  $4^{\circ}\text{C}$  for 30 min. Sca-1-negative cells were separated out using Dynal MPC-L Magnetic Particle Concentrators (Invitrogen), collected, and washed with sterile PBS. For BMT,  $1 \times 10^6$  Sca-1-depleted CD45.1 helper cells were mixed with each of the indicated test cell doses in Hanks' balanced salt solution (Gibco) and retro-orbitally injected into lethally irradiated CD45.1 Pepc/BoyJ recipient mice. Peripheral blood donor cell chimerism was analyzed at 4-week intervals after transplant for 16 weeks, and mice with at least 0.1% donor-descent (CD45.2) cells in the peripheral blood were counted as positive reconstitution (22). Stem cell frequency was estimated at the 16th week time point after transplantation using the ELDA.

### Quantification of intracellular LIPs

Human or mouse BMMNCs, as well as HPC7 cells, were incubated with 50 nM calcein-AM (Invitrogen) for 5 min at  $37^{\circ}\text{C}$ . Then, cells were washed with PBS and resuspended in prewarmed culture medium containing either the vehicle control ( $\text{H}_2\text{O}$ ) or EP (10 µg/ml) for 4 hours at  $37^{\circ}\text{C}$  and 5%  $\text{CO}_2$ . Intracellular calcein fluorescence was measured by flow cytometry on BD FACSAria II Special Order System (BD Biosciences), and MFI was calculated by FlowJo version 10.2 (FlowJo LLC).

### Measurement of intracellular ROS

Mouse BMMNCs were preloaded FAC (0 or 200 µg/ml) for 1 hour at  $37^{\circ}\text{C}$  before subjecting to liquid culture in MyeloCult M5300 (STEMCELL Technologies) supplemented with rmSCF (100 ng/ml; Gemini Bio-Products) for 1 hour at  $37^{\circ}\text{C}$  in the presence of vehicle control (NT),  $\text{H}_2\text{O}_2$  (200 µM), *N*-acetylcysteine (5 mM), or EP (10 µg/ml). The cells were washed in PBS and labeled with 2'-7'-dichlorodihydrofluorescein (DCF) diacetate (2.5 µM) fluorescent probe (Life Technologies) in the dark for 30 min at  $37^{\circ}\text{C}$ , followed by staining with antibodies against hematopoietic stem and progenitor cell markers (table S12) for 30 min at  $4^{\circ}\text{C}$  with light protection. DCF MFI values were obtained by flow cytometry and analyzed by FlowJo version 10.2 (FlowJo LLC).

### Complete blood counts

Peripheral blood was collected from the submandibular vein of living mice or the heart of euthanized mice and analyzed using the Forcyte Hematology Analyzer (Oxford Science Inc.) according to the manufacturer's instructions.

### Metabolomic profiling and analysis

For sample preparation, HPC7 cells treated with either vehicle ( $\text{H}_2\text{O}$ ) or EP (10 µg/ml) for 12 hours were harvested and washed with ice-cold

150 mM ammonium acetate at 4°C. Cells were then resuspended in 0.75 ml of ice-cold 150 mM ammonium acetate, transferred to chilled cryovials, and then centrifuged for 2 min at 4°C. The supernatant was removed, and the cell pellet was snap-frozen in liquid nitrogen and stored at -80°C until further processing. Metabolite extraction procedure was as previously described (81). Briefly, samples were added with 200 µl of methanol: H<sub>2</sub>O (4:1) containing three internal standards [U13\_succinate (2 nmol), U13\_citrate (1 nmol), and heptadecanoic acid (2 nmol)], followed by a 5-min sonication in ice water and snap-frozen in liquid nitrogen. Samples were then thawed on ice, followed by a 2-min sonication. The freeze-thaw-sonication procedure was repeated three times. After that, the samples were kept at -20°C for 10 min, followed by centrifugation at 12,000 rpm for 10 min. The supernatants were dried under gentle nitrogen flow and subsequently subjected to a two-step derivatization procedure. First, the samples were methoximized with 50 µl of methoxyamine hydrochloride (15 mg/ml in pyridine) at 30°C for 90 min. Then, the silylation step was done with 50 µl of *N,O*-bis(trimethylsilyl)trifluoroacetamide (containing 1% trimethylchlorosilane) at 70°C for 60 min. Samples were analyzed by gas chromatography time-of-flight mass spectrometry (GC-TOFMS; GCT Premier, Waters). The acquired GC-TOFMS data were processed using a ChromaTOF software (version 4.22; LECO Co.) as previously described (81). The data were normalized to internal standard (heptadecanoic acid) and cell number to obtain the relative quantification result. Metabolites with fold changes > 1.5 (EP versus NT) and *P* < 0.05 (Student's *t* test) were submitted for pathway enrichment analysis using hypergeometric test of MetaboAnalyst 3.0 (82).

## Statistics

The statistical significance of the difference between two groups of paired and unpaired samples was assessed by two-tailed Student's *t* test (paired and unpaired, respectively, as specified in the figure legends). Prism 7.0 [GraphPad Software (www.graphpad.com)] was used for statistical analyses and plotting of bar graphs. Differential expression analysis was performed with limma Bioconductor package (74), and hypergeometric test was performed with the built-in phyper function of R. Statistical significance for estimation of stem cell frequency in LTC-IC and limiting dilution-competitive BMT assays was tested with ELDA method in the statmod package of R (80).

## SUPPLEMENTARY MATERIALS

www.sciencetranslationalmedicine.org/cgi/content/full/10/458/eaas9563/DC1

Fig. S1. Effects of EP on human MPP cells.

Fig. S2. Effects of EP on cell cycling of HSCs.

Fig. S3. Alterations of iron-associated gene expression in human hematopoietic cells after EP treatment.

Fig. S4. TPO-R-independent stimulation of HSC self-renewal by EP.

Fig. S5. Reduction of HSCs in *c-Mpl*<sup>-/-</sup> mice.

Fig. S6. Complete blood counts of *c-Mpl*<sup>-/-</sup> mice after in vivo treatment with EP.

Fig. S7. Alterations of glycolysis-associated genes in mouse HSCs after EP treatment.

Fig. S8. FAC dose finding for ex vivo assays.

Fig. S9. Intracellular ROS concentrations in HSCs after EP treatment.

Fig. S10. Iron-dependent HSC self-renewal upon chelator treatment.

Fig. S11. Iron-associated gene expression changes in ITP patients treated with EP.

Table S1. DEGs in TPO-treated human HSCs.

Table S2. DEGs in EP-treated human HSCs.

Table S3. Commonly altered DEGs between EP- and TPO-treated human HSCs.

Table S4. IPA analysis with DEGs specifically detected in EP-treated human HSCs.

Table S5. Plasma concentrations of EP in mice.

Table S6. DEGs in EP-treated mouse HSCs.

Table S7. IPA analysis with DEGs in EP-treated mouse HSCs.

Table S8. Altered metabolites detected in EP-treated HPC7 cells.

Table S9. Pathway analysis with altered metabolites detected in EP-treated HPC7 cells.

Table S10. IPA analysis with altered metabolites detected in EP-treated HPC7 cells.

Table S11. Information on primary human-derived specimens.

Table S12. List of antibodies used in FACS experiments.

Table S13. List of primers for qPCR.

## REFERENCES AND NOTES

- F. Rodeghiero, R. Stasi, T. Gernsheimer, M. Michel, D. Provan, D. M. Arnold, J. B. Bussel, D. B. Cines, B. H. Chong, N. Cooper, B. Godeau, K. Lechner, M. G. Mazzucconi, R. McMillan, M. A. Sanz, P. Imbach, V. Blanchette, T. Kühne, M. Ruggeri, J. N. George, Standardization of terminology, definitions and outcome criteria in immune thrombocytopenic purpura of adults and children: Report from an international working group. *Blood* **113**, 2386–2393 (2009).
- D. B. Cines, V. S. Blanchette, Immune thrombocytopenic purpura. *N. Engl. J. Med.* **346**, 1923 (2002).
- N. S. Young, J. Maciejewski, The pathophysiology of acquired aplastic anemia. *N. Engl. J. Med.* **336**, 1365–1372 (1997).
- S. J. Corey, Mark D. Minden, D. L. Barber, H. Kantarjian, J. C. Y. Wang, A. D. Schimmer, Myelodysplastic syndromes: The complexity of stem-cell diseases. *Nat. Rev. Cancer* **7**, 118–129 (2007).
- K. Kaushansky, The molecular mechanisms that control thrombopoiesis. *J. Clin. Invest.* **115**, 3339–3347 (2005).
- H. Qian, N. Buza-Vidas, C. D. Hyland, C. T. Jensen, J. Antonchuk, R. Månsson, L. A. Thoren, M. Ekblom, W. S. Alexander, S. E. W. Jacobsen, Critical role of thrombopoietin in maintaining adult quiescent hematopoietic stem cells. *Cell Stem Cell* **1**, 671–684 (2007).
- H. Yoshihara, F. Arai, K. Hosokawa, T. Hagiwara, K. Takubo, Y. Nakamura, Y. Gomei, H. Iwasaki, S. Matsuoka, K. Miyamoto, H. Miyazaki, T. Takahashi, T. Suda, Thrombopoietin/MPL signaling regulates hematopoietic stem cell quiescence and interaction with the osteoblastic niche. *Cell Stem Cell* **1**, 685–697 (2007).
- D. J. Kuter, C. G. Begley, Recombinant human thrombopoietin: Basic biology and evaluation of clinical studies. *Blood* **100**, 3457–3469 (2002).
- R. L. Bassor, E. O'Flaherty, M. Green, M. Edmonds, J. Nichol, D. M. Menchaca, B. Cohen, C. Glenn Begley, Development of pancytopenia with neutralizing antibodies to thrombopoietin after multicycle chemotherapy supported by megakaryocyte growth and development factor. *Blood* **99**, 2599–2602 (2002).
- C. L. Erickson-Miller, E. Delorme, S.-S. Tian, C. B. Hopson, A. J. Landis, E. I. Valoret, T. S. Sellers, J. Rosen, S. G. Miller, J. I. Luengo, K. J. Duffy, J. M. Jenkins, Preclinical activity of eltrombopag (SB-497115), an oral, nonpeptide thrombopoietin receptor agonist. *Stem Cells* **27**, 424–430 (2009).
- B. Will, M. Kawahara, J. P. Luciano, I. Bruns, S. Parekh, C. L. Erickson-Miller, M. A. Aivado, A. Verma, U. Steidl, Effect of the nonpeptide thrombopoietin receptor agonist eltrombopag on bone marrow cells from patients with acute myeloid leukemia and myelodysplastic syndrome. *Blood* **114**, 3899–3908 (2009).
- C. L. Erickson-Miller, E. De Lorme, S.-S. Tian, C. B. Hopson, K. Stark, L. Giampa, E. I. Valoret, K. J. Duffy, J. L. Luengo, J. Rosen, S. G. Miller, S. B. Dillon, P. Lamb, Discovery and characterization of a selective, nonpeptidyl thrombopoietin receptor agonist. *Exp. Hematol.* **33**, 85–93 (2005).
- L. Boiocchi, A. Orazi, W. Ghanima, M. Arabadjief, J. B. Bussel, J. T. Geyer, Thrombopoietin receptor agonist therapy in primary immune thrombocytopenia is associated with bone marrow hypercellularity and mild reticuline fibrosis but not other stromal abnormalities. *Mod. Pathol.* **25**, 65–74 (2012).
- M. J. Olnes, Eltrombopag can stimulate trilineage hematopoiesis with transfusion independence in patients with refractory severe aplastic anemia: Results from a phase II trial, in *ASH Annual Meeting Abstracts*, San Diego Convention Center, 10 to 13 December 2011.
- R. Desmond, D. M. Townsley, B. Dumitriu, M. J. Olnes, P. Scheinberg, M. Bevans, A. R. Parikh, K. Broder, K. R. Calvo, C. O. Wu, N. S. Young, C. E. Dunbar, Eltrombopag restores trilineage hematopoiesis in refractory severe aplastic anemia that can be sustained on discontinuation of drug. *Blood* **123**, 1818–1825 (2014).
- M. J. Olnes, P. Scheinberg, K. R. Calvo, R. Desmond, Y. Tang, B. Dumitriu, A. R. Parikh, S. Soto, A. Biancotto, X. Feng, J. Lozier, C. O. Wu, N. S. Young, C. E. Dunbar, Eltrombopag and improved hematopoiesis in refractory aplastic anemia. *N. Engl. J. Med.* **367**, 11–19 (2012).
- M. Roth, B. Will, G. Simkin, S. Narayanagari, L. Barretero, B. Bartholdy, R. Tamari, C. S. Mitsiades, A. Verma, U. Steidl, Eltrombopag inhibits the proliferation of leukemia cells via reduction of intracellular iron and induction of differentiation. *Blood* **120**, 386–394 (2012).
- E. Vlachodimitropoulou, Y.-L. Chen, M. Garbowski, P. Koonyosying, B. Psaila, M. Sola-Visner, N. Cooper, R. Hider, J. Porter, Eltrombopag: A powerful chelator of cellular or extracellular iron(III) alone or combined with a second chelator. *Blood* **130**, 1923–1933 (2017).
- M. U. Muckenthaler, B. Galy, M. W. Hentze, Systemic iron homeostasis and the iron-responsive element/iron-regulatory protein (IRE/IRP) regulatory network. *Annu. Rev. Nutr.* **28**, 197–213 (2008).

20. A. L. Gurney, K. Carver-Moore, F. J. de Sauvage, M. W. Moore, Thrombocytopenia in c-mpl-deficient mice. *Science* **265**, 1445–1447 (1994).
21. A. Bersenev, C. Wu, J. Balcerak, W. Tong, Lnk controls mouse hematopoietic stem cell self-renewal and quiescence through direct interactions with JAK2. *J. Clin. Invest.* **118**, 2832–2844 (2008).
22. S. J. Szilvassy, R. K. Humphries, P. M. Lansdorf, A. C. Eaves, C. J. Eaves, Quantitative assay for totipotent reconstituting hematopoietic stem cells by a competitive repopulation strategy. *Proc. Natl. Acad. Sci. U.S.A.* **87**, 8736–8740 (1990).
23. P. Pinto do Ó, Å. Kolterud, L. Carlsson, Expression of the LIM-homeobox gene *LH2* generates immortalized Steel factor-dependent multipotent hematopoietic precursors. *EMBO J.* **17**, 5744–5756 (1998).
24. A. Kalota, M. A. Selak, L. A. Garcia-Cid, M. Carroll, Eltrombopag modulates reactive oxygen species and decreases acute myeloid leukemia cell survival. *PLOS ONE* **10**, e0126691 (2015).
25. J. P. Adjimani, P. Asare, Antioxidant and free radical scavenging activity of iron chelators. *Toxicol. Rep.* **2**, 721–728 (2015).
26. S. J. Dixon, B. R. Stockwell, The role of iron and reactive oxygen species in cell death. *Nat. Chem. Biol.* **10**, 9–17 (2014).
27. J. C. Robinson, B. B. Graham, T. C. Rouault, R. M. Tudor, The crossroads of iron with hypoxia and cellular metabolism implications in the pathobiology of pulmonary hypertension. *Am. J. Respir. Cell Mol. Biol.* **51**, 721–729 (2014).
28. C. Peyssonnaud, A. S. Zinkernagel, R. A. Schuepbach, E. Rankin, S. Vaulont, V. H. Haase, V. Nizet, R. S. Johnson, Regulation of iron homeostasis by the hypoxia-inducible transcription factors (HIFs). *J. Clin. Invest.* **117**, 1926–1932 (2007).
29. I. Siegert, J. Schödel, M. Nairz, V. Schatz, K. Dettmer, C. Dick, J. Kalucka, K. Franke, M. Ehrenschwender, G. Schley, A. Beneke, J. Sutter, M. Moll, C. Hellerbrand, B. Wielockx, D. M. Katschinski, R. Lang, B. Galy, M. W. Hentze, P. Koivunen, P. J. Oefner, C. Bogdan, G. Weiss, C. Willam, Ferritin-mediated iron sequestration stabilizes hypoxia-inducible factor-1 $\alpha$  upon LPS activation in the presence of ample oxygen. *Cell Rep.* **13**, 2048–2055 (2015).
30. R. Sood, W. Wong, M. Jeng, J. L. Zehnder, Gene expression profile of idiopathic thrombocytopenic purpura (ITP). *Pediatr. Blood Cancer* **47**, 675–677 (2006).
31. B. Zhang, C. Lo, L. Shen, R. Sood, C. Jones, K. Cusmano-Ozog, S. Park-Snyder, W. Wong, M. Jeng, T. Cowan, E. G. Engleman, J. L. Zehnder, The role of vanin-1 and oxidative stress-related pathways in distinguishing acute and chronic pediatric ITP. *Blood* **117**, 4569–4579 (2011).
32. D. M. Townsley, P. Scheinberg, T. Winkler, R. Desmond, B. Dumitriu, O. Rios, B. Weinstein, J. Valdez, J. Lotter, X. Feng, M. Desierto, H. Leuva, M. Bevans, C. Wu, A. Larochelle, K. R. Calvo, C. E. Dunbar, N. S. Young, Eltrombopag added to standard immunosuppression for aplastic anemia. *N. Engl. J. Med.* **376**, 1540–1550 (2017).
33. F. Notta, S. Doulatov, E. Laurenti, A. Poepl, I. Jurisica, J. E. Dick, Isolation of single human hematopoietic stem cells capable of long-term multilineage engraftment. *Science* **333**, 218–221 (2011).
34. I. Matsumura, Y. Kanakura, T. Kato, H. Ikeda, J. Ishikawa, Y. Horikawa, K. Hashimoto, Y. Moriyama, T. Tsujimura, T. Nishiura, Growth response of acute myeloblastic leukemia cells to recombinant human thrombopoietin. *Blood* **86**, 703–709 (1995).
35. D. D. Williams, B. Peng, C. K. Bailey, M. B. Wire, Y. Deng, J. W. Park, D. A. Collins, S. G. Kapsi, J. M. Jenkins, Effects of food and antacids on the pharmacokinetics of eltrombopag in healthy adult subjects: Two single-dose, open-label, randomized-sequence, crossover studies. *Clin. Ther.* **31**, 764–776 (2009).
36. M. B. Wire, J. Bruce, J. Gauvin, C. J. Pendry, S. M. Guire, Y. Qian, A randomized, open-label, 5-period, balanced crossover study to evaluate the relative bioavailability of eltrombopag powder for oral suspension (PFOS) and tablet formulations and the effect of a high-calcium meal on eltrombopag pharmacokinetics when administered with or 2 hours before or after PFOS. *Clin. Ther.* **34**, 699–709 (2012).
37. I. Bauer, H.-J. Knölker, Iron catalysis in organic synthesis. *Chem. Rev.* **115**, 3170–3387 (2015).
38. R. Lill, Function and biogenesis of iron-sulphur proteins. *Nature* **460**, 831–838 (2009).
39. T. L. Poulos, Heme enzyme structure and function. *Chem. Rev.* **114**, 3919–3962 (2014).
40. L. M. Bystrom, M. L. Guzman, S. Rivella, Iron and reactive oxygen species: Friends or foes of cancer cells? *Antioxid. Redox Signal.* **20**, 1917–1924 (2014).
41. T. W. Bastian, K. A. Duck, G. C. Michalopoulos, M. J. Chen, Z.-J. Liu, J. R. Connor, L. M. Lanier, M. C. Sola-Visner, M. K. Georgeff, Eltrombopag, a thrombopoietin mimetic, crosses the blood-brain barrier and impairs iron-dependent hippocampal neuron dendrite development. *J. Thromb. Haemost.* **15**, 565–574 (2017).
42. M. P. Lambert, C. M. Witmer, J. L. Kwiatkowski, Therapy induced iron deficiency in children treated with eltrombopag for immune thrombocytopenia. *Am. J. Hematol.* **92**, E88–E91 (2017).
43. J. B. Bussel, P. G. Miguel, J. M. Despotovic, J. D. Grainger, J. Sevilla, V. S. Blanchette, L. Krishnamurti, P. Connor, M. David, K. B. Boayeg, D. C. Matthews, M. P. Lambert, L. M. Marcelllo, M. Iyengar, G. W. Chan, K. D. Chagin, D. Theodore, C. K. Bailey, Eltrombopag for the treatment of children with persistent and chronic immune thrombocytopenia (PETIT): A randomised, multicentre, placebo-controlled study. *Lancet Haematol.* **2**, e315–e325 (2015).
44. J. D. Grainger, F. Locatelli, T. Chotsamcharoen, E. Donyush, B. Pongtanakul, Patcharee Komvilaisak, D. Sosothikul, G. Drelichman, N. Sirachainan, S. Holzhauser, V. Lebedev, R. Lemons, D. Pospisilova, U. Ramenghi, J. B. Bussel, Kalna K. Bakshi, M. Iyengar, G. W. Chan, K. D. Chagin, D. Theodore, L. M. Marcelllo, C. K. Bailey, Eltrombopag for children with chronic immune thrombocytopenia (PETIT2): A randomised, multicentre, placebo-controlled trial. *Lancet* **386**, 1649–1658 (2015).
45. D. J. R. Lane, A. M. Merlot, M. L.-H. Huang, D.-H. Bae, P. J. Jansson, S. Sahni, D. S. Kalinowski, D. R. Richardson, Cellular iron uptake, trafficking and metabolism: Key molecules and mechanisms and their roles in disease. *BBA Mol. Cell. Res.* **1853**, 1130–1144 (2015).
46. C. Pigeon, G. Ilyin, B. Courselaud, P. Leroyer, B. Turlin, P. Brissot, O. Lóréal, A new mouse liver-specific gene, encoding a protein homologous to human antimicrobial peptide hepcidin, is overexpressed during iron overload. *J. Biol. Chem.* **276**, 7811–7819 (2001).
47. K. Pantopoulos, G. Weiss, M. W. Hentze, Nitric oxide and oxidative stress (H<sub>2</sub>O<sub>2</sub>) control mammalian iron metabolism by different pathways. *Mol. Cell. Biol.* **16**, 3781–3788 (1996).
48. S. Silva-Gomes, C. Bouton, T. Silva, P. Santambrogio, P. Rodrigues, R. Appelberg, M. S. Gomes, *Mycobacterium avium* infection induces H-ferritin expression in mouse primary macrophages by activating Toll-like receptor 2. *PLOS ONE* **8**, e82874 (2013).
49. C. Bouton, M.-J. Chauveau, S. Lazereg, J.-C. Drapier, Recycling of RNA binding iron regulatory protein 1 into an aconitase after nitric oxide removal depends on mitochondrial ATP. *J. Biol. Chem.* **277**, 31220–31227 (2002).
50. M. C. Sammarco, S. Ditch, A. Banerjee, E. Grabczyk, Ferritin L and H subunits are differentially regulated on a post-transcriptional level. *J. Biol. Chem.* **283**, 4578–4587 (2008).
51. L. H. Fell, S. Seiler-Muñler, A. B. Sellier, B. Rotter, Peter WinterMartina Sester, D. Fliser, G. H. Heine, A. M. Zawada, Impact of individual intravenous iron preparations on the differentiation of monocytes towards macrophages and dendritic cells. *Nephrol. Dial. Transplant.* **31**, 1835–1845 (2016).
52. P. Matak, A. Matak, S. Moustafa, D. K. Aryal, E. J. Benner, W. Wetsel, N. C. Andrews, Disrupted iron homeostasis causes dopaminergic neurodegeneration in mice. *Proc. Natl. Acad. Sci. U.S.A.* **113**, 3428–3435 (2016).
53. G. F. Vile, S. Basu-Modak, C. Waltner, R. M. Tyrrell, Heme oxygenase-1 mediates an adaptive response to oxidative stress in human skin fibroblasts. *Proc. Natl. Acad. Sci. U.S.A.* **91**, 2607–2610 (1994).
54. E. V. Koumoutsea, N. Cooper, B. Psaila, M. Sola-Visner, J. B. Porter, Eltrombopag mobilizes intracellular iron stores at concentrations lower than those required with other clinically available iron chelators. *Blood* **124**, 1353 (2014).
55. E. V. Koumoutsea, J. B. Porter, N. Cooper, B. Psaila, M. Sola-Visner, A potential novel application of eltrombopag: A combination agent to enhance iron chelation therapy. *Blood* **126**, 3357 (2015).
56. C. C. Winterbourn, Toxicity of iron and hydrogen peroxide: The Fenton reaction. *Toxicol. Lett.* **82–83**, 969–974 (1995).
57. F. R. Vargas, Y. Diaz, K. Carbonell, Antioxidant and scavenging activity of emodin, aloe-emodin, and rhein on free-radical and reactive oxygen species. *Pharm. Biol.* **42**, 342–348 (2004).
58. K. Takubo, N. Goda, W. Yamada, H. Iriuchishima, E. Ikeda, Y. Kubota, H. Shima, R. S. Johnson, A. Hirao, M. Suematsu, T. Suda, Regulation of the HIF-1 $\alpha$  level is essential for hematopoietic stem cells. *Cell Stem Cell* **7**, 391–402 (2010).
59. T. Uchida, F. Rossignol, M. A. Matthay, R. Mounier, S. Couette, E. Clottes, C. Clerici, Prolonged hypoxia differentially regulates hypoxia-inducible factor (HIF)-1 $\alpha$  and HIF-2 $\alpha$  expression in lung epithelial cells: Implication of natural antisense HIF-1 $\alpha$ . *J. Biol. Chem.* **279**, 14871–14878 (2004).
60. R. Pascal, A. Pross, J. D. Sutherland, Towards an evolutionary theory of the origin of life based on kinetics and thermodynamics. *Open Biol.* **3**, 130156 (2013).
61. H. I. Nakada, S. Weinhouse, Non-enzymatic transamination with glyoxylic acid and various amino acids. *J. Biol. Chem.* **204**, 831–836 (1953).
62. T. H. Siddall, W. E. Stewart, Proton magnetic resonance studies of rotational isomerism around the 2-propyl-nitrogen bond in some thionamides. *J. Org. Chem.* **35**, 1019–1022 (1970).
63. R. W. Gracy, E. A. Noltmann, Studies on phosphomannose isomerase III. A mechanism for catalysis and for the role of zinc in the enzymatic and the nonenzymatic isomerization. *J. Biol. Chem.* **243**, 5410–5419 (1968).
64. M. A. Keller, A. Zylstra, C. Castro, A. V. Turczyn, J. L. Griffin, M. Ralsler, Conditional iron and pH-dependent activity of a non-enzymatic glycolysis and pentose phosphate pathway. *Sci. Adv.* **2**, e1501235 (2016).
65. A. Krzyżaniak, J. Balciszwski, P. Salański, J. Jurczak, The non-enzymatic specific aminoacylation of transfer RNA at high pressure. *Int. J. Biol. Macromol.* **16**, 153–158 (1994).

66. P. A. Frey, The Leloir pathway: A mechanistic imperative for three enzymes to change the stereochemical configuration of a single carbon in galactose. *FASEB J.* **10**, 461–470 (1996).
67. H.-S. Kim, C. Xiao, R.-H. Wang, T. Lahusen, X. Xu, A. Vassilopoulos, G. Vazquez-Ortiz, W.-I. Jeong, O. Park, S. H. Ki, B. Gao, C.-X. Deng, Hepatic-specific disruption of SIRT6 in mice results in fatty liver formation due to enhanced glycolysis and triglyceride synthesis. *Cell Metab.* **12**, 224–236 (2010).
68. D. Nakada, T. L. Saunders, S. J. Morrison, Lkb1 regulates cell cycle and energy metabolism in haematopoietic stem cells. *Nature* **468**, 653–658 (2010).
69. S. Gurumurthy, S. Z. Xie, B. Alagesan, J. Kim, R. Z. Yusuf, B. Saez, A. Tzatsos, F. Ozsolak, P. Milos, F. Ferrari, P. J. Park, O. S. Shirihai, D. T. Scadden, N. Bardeesy, The Lkb1 metabolic sensor maintains haematopoietic stem cell survival. *Nature* **468**, 659–663 (2010).
70. B. Gan, J. Hu, S. Jiang, Y. Liu, E. Sahin, L. Zhuang, E. Fletcher-Sananikone, S. Colla, Y. A. Wang, L. Chin, R. A. DePinho, Lkb1 regulates quiescence and metabolic homeostasis of haematopoietic stem cells. *Nature* **468**, 701–704 (2010).
71. J. Huang, M. Nguyen-McCarthy, E. O. Hexner, G. Danet-Desnoyers, P. S. Klein, Maintenance of hematopoietic stem cells through regulation of Wnt and mTOR pathways. *Nat. Med.* **18**, 1778–1785 (2012).
72. A. V. Guitart, T. I. Panagopoulou, A. Villacreces, M. Vukovic, C. Sepulveda, L. Allen, R. N. Carter, L. N. van de Lagemaat, M. Morgan, P. Giles, Z. Sas, M. V. Gonzalez, H. Lawson, J. Paris, J. Edwards-Hicks, K. Schaak, C. Subramani, D. Gezer, A. Armesilla-Diaz, J. Wills, A. Easterbrook, D. Coman, C. W. E. So, Donal O'Carroll, D. Vernimmen, N. P. Rodrigues, P. J. Pollard, N. M. Morton, A. Finch, K. R. Kranc, Fumarate hydratase is a critical metabolic regulator of hematopoietic stem cell functions. *J. Exp. Med.* **214**, 719–735 (2017).
73. B. S. Carvalho, R. A. Irizarry, A framework for oligonucleotide microarray preprocessing. *Bioinformatics* **26**, 2363–2367 (2010).
74. M. E. Ritchie, B. Phipson, D. Wu, Y. Hu, C. W. Law, W. Shi, G. K. Smyth, *limma* powers differential expression analyses for RNA-sequencing and microarray studies. *Nucleic Acids Res.* **43**, e47 (2015).
75. M. Campillos, I. Cases, M. W. Hentze, M. Sanchez, SIREs: Searching for iron-responsive elements. *Nucleic Acids Res.* **38**, W360–W367 (2010).
76. N. A. O'Leary, M. W. Wright, J. Rodney Brister, S. Ciufu, D. Haddad, R. McVeigh, B. Rajput, B. Robbertse, B. Smith-White, D. Ako-Adjei, A. Astashyn, A. Badretdin, Y. Bao, O. Blinkova, V. Brover, V. Chetvermin, J. Choi, E. Cox, O. Ermolaeva, C. M. Farrell, T. Goldfarb, T. Gupta, D. Haft, E. Hatcher, W. Hlavina, V. S. Joardar, V. K. Kodali, W. Li, D. Maglott, P. Masterson, K. M. McGarvey, M. R. Murphy, Kathleen O'Neill, S. Pujar, S. H. Rangwala, D. Rausch, L. D. Riddick, C. Schoch, A. Shkeda, S. S. Storz, H. Sun, F. Thibaud-Nissen, I. Tolstoy, R. E. Tully, A. R. Vatsan, C. Wallin, D. Webb, W. Wu, M. J. Landrum, A. Kimchi, T. Tatusova, M. DiCuccio, P. Kitts, T. D. Murphy, K. D. Pruitt, Reference sequence (RefSeq) database at NCBI: Current status, taxonomic expansion, and functional annotation. *Nucleic Acids Res.* **44**, D733–D745 (2016).
77. J. T. Leek, W. E. Johnson, H. S. Parker, A. E. Jaffe, J. D. Storey, The *sva* package for removing batch effects and other unwanted variation in high-throughput experiments. *Bioinformatics* **28**, 882–883 (2012).
78. W. E. Johnson, C. Li, A. Rabinovic, Adjusting batch effects in microarray expression data using empirical Bayes methods. *Biostatistics* **8**, 118–127 (2007).
79. C. L. Miller, B. Dykstra, C. J. Eaves, Characterization of mouse hematopoietic stem and progenitor cells. *Curr. Protoc. Immunol.* **80**, 22B.2.1–22B.2.31 (2008).
80. Y. Hu, G. K. Smyth, ELDA: Extreme limiting dilution analysis for comparing depleted and enriched populations in stem cell and other assays. *J. Immunol. Methods* **347**, 70–78 (2009).
81. L. Pan, Y. Qiu, T. Chen, J. Lin, Y. Chi, M. Su, A. Zhao, W. Jia, An optimized procedure for metabonomic analysis of rat liver tissue using gas chromatography/time-of-flight mass spectrometry. *J. Pharm. Biomed. Anal.* **52**, 589–596 (2010).
82. J. Xia, I. Sinelnikov, B. Han, D. Wishart, MetaboAnalyst 3.0—Making metabolomics more meaningful. *Nucleic Acids Res.* **43**, W251–W257 (2015).

**Acknowledgments:** We are thankful to W. Tong for providing *Mpl*-deficient mice and O. Abdel-Wahab for providing the mouse MPP cell line HPC7. We further thank D. Sun from the Einstein Stem Cell Isolation and Xenotransplantation Facility (funded through New York Stem Cell Science grant C029154) for expert assistance with flow cytometry and D. Reynolds and W. Tran from the Einstein Genomics Core Facility for help with the microarray experiments. For metabolite profiling assays, we thank Y. Qiu and I. Kurland from the Stable Isotope and Metabolomics Core Facility of the Einstein-Mount Sinai Diabetes Research Center of the Albert Einstein College of Medicine (supported by NIH/National Cancer Institute grant P60DK020541) for expert support. We also thank P. Schultes from the Department of Cell Biology at Albert Einstein College of Medicine for expert technical assistance. We thank the team members of the Will and Steidl Laboratories, as well as M. Roth for helpful discussions. **Funding:** This work was supported by K01DK105134 (to B.W.), P30CA013330 (pilot grant; to B.W.), R01CA166429 (to U.S.), R01CA217092 (to U.S.), and the Einstein Training Program in Stem Cell Research from the Empire State Stem Cell Fund through New York State Department of Health Contract C30292GG (to J.C. and M.M.A.). U.S. is a research scholar of the Leukemia and Lymphoma Society and the Diane and Arthur B. Belfer Faculty Scholar in Cancer Research of the Albert Einstein College of Medicine. **Author contributions:** B.W. and U.S. designed the research. Y.-R.K. and B.W. designed the experiments. Y.-R.K., J.C., S.-R.N., T.I.T., M.M.A., and M.F. performed the experiments. Y.-R.K. and J.C. performed the bioinformatical analysis of data. All authors interpreted the data. J.B.B., A.S., I.M., and A.V. provided the patient specimen. Y.-R.K. and B.W. wrote the manuscript. **Competing interests:** B.W., U.S., and A.V. have received research support from GlaxoSmithKline and Novartis Pharmaceuticals. B.W., U.S., and A.V. have served as consultants for Novartis Pharmaceuticals. P.M.R. and C.P. are employees of Novartis Pharmaceuticals. J.B.B. has served as a consultant on advisory medical and scientific boards for Amgen, Novartis, Rigel, Momenta, and Union Chimique Belge (U.C.B.). Although J.B.B. has been consulting for Novartis and Rigel, he has had no role in arranging purchases of pharmaceuticals. **Data and materials availability:** All data associated with this study are present in the paper or the Supplementary Materials. Gene expression microarray data for this study have been deposited in Gene Expression Omnibus database with accession number GSE107430.

Submitted 16 January 2018  
Resubmitted 13 June 2018  
Accepted 22 August 2018  
Published 12 September 2018  
10.1126/scitranslmed.aas9563

**Citation:** Y.-R. Kao, J. Chen, S.-R. Narayanagari, T. I. Todorova, M. M. Aivalioti, M. Ferreira, P. M. Ramos, C. Pallaud, I. Mantzaris, A. Shastri, J. B. Bussel, A. Verma, U. Steidl, B. Will, Thrombopoietin receptor-independent stimulation of hematopoietic stem cells by eltrombopag. *Sci. Transl. Med.* **10**, eaas9563 (2018).

## Thrombopoietin receptor–independent stimulation of hematopoietic stem cells by eltrombopag

Yun-Ruei Kao, Jiahao Chen, Swathi-Rao Narayanagari, Tihomira I. Todorova, Maria M. Aivalioti, Mariana Ferreira, Pedro M. Ramos, Celine Pallaud, Ioannis Mantzaris, Aditi Shastri, James B. Bussel, Amit Verma, Ulrich Steidl, and Britta Will

*Sci. Transl. Med.*, **10** (458), eaas9563.  
DOI: 10.1126/scitranslmed.aas9563

### Ironing out bone marrow failure

Chronic thrombocytopenia can be associated with a variety of conditions, such as bone marrow failure syndromes and immune disorders. It increases the risk of severe bleeding, and therapies such as platelet transfusion or recombinant thrombopoietin are associated with a variety of complications. In contrast, the small-molecule eltrombopag, a thrombopoietin receptor agonist, has been very effective in treating thrombocytopenia in patients with bone marrow failure. Kao *et al.* demonstrated that, in addition to targeting the thrombopoietin receptor, eltrombopag also chelates iron and that this chelating action enables it to improve the function of bone marrow stem cells. The authors also determined the mechanism linking iron chelation to hematopoietic stem cell maintenance, which may help facilitate the development of future treatments.

### View the article online

<https://www.science.org/doi/10.1126/scitranslmed.aas9563>

### Permissions

<https://www.science.org/help/reprints-and-permissions>

Use of this article is subject to the [Terms of service](#)